UNIVERSAL WISER
PUBLISHER

Research Article

Improved Shear-Lag Analytical Model for Mixed Adhesive Double Lap Joint

Mikel Al-Hayek [iD]**, Georges Challita**[*] [iD]

MMC, CRSI, Lebanese University, Faculty of Engineering, Roumieh, El-Metn, Lebanon
Email: georges.challita@ul.edu.lb

Abstract: In the present work, the improved shear-lag model based on a linear shear stress distribution in the substrates' thickness of a mixed-adhesive double-lap joint (MADLJ) has been developed to establish the shear stress profile along the joint length. A closed-form solution has been obtained and numerically validated by a 2D finite element simulation carried out on ABAQUS CAE commercial software. The analytical model has been then employed to conduct a parametric study where the influences of the stiff and soft adhesives Young moduli, their lengths as well as the joint's thickness on the maximum shear stress in the joint have been examined, and this for seven different substrate's thicknesses. Many key values of those parameters defining the transition of maximum shear stress from stiff to a soft region or defining an optimum stress or a limit value where the pure joint becomes advantageous along with their evolution with the adherents' thicknesses have been determined.

Keywords: mixed-adhesive joint, improved shear-lag, adhesive shear, finite element analysis

Abbreviation

SLJ	Single Lap Joint
DLJ	Double Lap Joint
MAJ	Mixed-Adhesive Joint
MADLJ	Mixed-Ad hesive Double Lap Joint
CFHO	Closed-Form High Order
FEM	Finite Element Method

Symbol

a	Length of the soft adhesive in region (1)
b	Length of the stiff adhesive in region (2)
c	Length of the soft adhesive in region (3)
t_o	Thickness of the outer adherent

t_i	Thickness of the inner adherent
t_a	Thickness of the adhesive layer
E_o	Young's modulus of the outer adherent
E_i	Young's modulus of the inner adherent
G_o	Shear modulus of the outer adherent
G_i	Shear modulus of the inner adherent
G_{a1}	Shear modulus of the adhesive layer in region (1)
G_{a2}	Shear modulus of the adhesive layer in region (2)
G_{a3}	Shear modulus of the adhesive layer in region (3)
$u_{o(1)}$	Axial displacement in region (1) of the outer adherent
$u_{i(1)}$	Axial displacement in region (1) of the inner adherent
$\langle u_{o(1)} \rangle$	Average axial displacement in region (1) of the outer adherent
$\langle u_{i(1)} \rangle$	Average axial displacement in region (1) of the inner adherent
$\langle u_{o(2)} \rangle$	Average axial displacement in region (2) of the outer adherent
$\langle u_{i(2)} \rangle$	Average axial displacement in region (2) of the inner adherent
$\langle u_{o(3)} \rangle$	Average axial displacement in region (3) of the outer adherent
$\langle u_{i(3)} \rangle$	Average axial displacement in region (3) of the inner adherent
$u_{io(1)}$	Interfacial axial displacement in region (1) outer adherent-adhesive
$u_{ii(1)}$	Interfacial axial displacement in region (1) inner adherent-adhesive
$u_{to(1)}$	Axial displacement in region (1) at the top surface of the outer adherent
$\sigma_{o(1)}$	Axial normal stress in region (1) of the outer adherent
$\sigma_{i(1)}$	Axial normal stress in region (1) of the inner adherent
$\tau_{o(1)}$	Through-thickness shear stress in region (1) of the outer adherent
$\tau_{i(1)}$	Through-thickness shear stress in region (1) of the inner adherent
$\tau_{a(1)}$	Adhesive shear stress in region (1)
$\tau_{a(2)}$	Adhesive shear stress in region (2)
$\tau_{a(3)}$	Adhesive shear stress in region (3)
$\gamma_{o(1)}$	Through-thickness shear strain in region (1) of the outer adherent
$\gamma_{i(1)}$	Through-thickness shear strain in region (1) of the inner adherent
$\gamma_{a(1)}$	Adhesive shear strain in region (1)
$T_{o(1)}$	Axial force per unit width in region (1) of the outer adherent
$T_{i(1)}$	Axial force per unit width in region (1) of the inner adherent
$T_{o(2)}$	Axial force per unit width in region (2) of the outer adherent
$T_{i(2)}$	Axial force per unit width in region (2) of the inner adherent
$T_{o(3)}$	Axial force per unit width in region (3) of the outer adherent
$T_{i(3)}$	Axial force per unit width in region (3) of the inner adherent
P_0	External axial force applied at the right end of the inner adherent
α	Homogeneity of shear stress
S_{max}	Maximum normalized shear stress to average stress

1. Introduction

For a couple of decades, the adhesive bonding technique has been intended to replace traditional joining methods such as screwing, riveting, or welding as it provides lightness to structures, as well as the stress distribution along wider

surfaces and the absence of disruptions in the substrates. This has offered mainly a huge advantage for assemblies used in transportation means and above all to the bond core to skins in sandwich panels [1]-[3]. Different techniques have been applied by researchers to well understand the behavior of these joints relying either on numerical, experimental, and analytical approaches or any combination of them. Despite the numerous advantages offered by this joining technique, adhesive joints endure the existence of stress peaks at the neighborhood of the joint's ends. Globally this aspect could be assessed through either numerical or analytical models.

Despite the fact that analytical solutions are laborious, they can be simply implemented and are considerably time-saving particularly when investigating a wide range of parameters. Historically speaking, one of the first analytical models describing the behavior of a bonded lap joint was established by Volkersen [4] who proposed a closed-form solution of the shear stress developed in a single lap joint (SLJ) based on the classical shear-lag model (differential shear). The non-linear geometric deformation of an SLJ was analyzed by Goland and Reissner [5] where a closed-form solution for shear and peel stress distribution along the overlap was found; this latter has been improved by the model of Hart-Smith [6] considering elasto-plastic behavior of the adhesive for both SLJ and DLJ geometries. Allman [7] adopted the elastic theory through which the effect of bending, stretching, and shearing of adherent (isotropic and composite) and the shearing and tearing of adhesive were studied on SLJ as well as DLJ. He spotted the location of the peak of stress in the joint and its dependency on the relative stiffness between the adhesive and the adherents. One of the most interesting models has been developed by Bigwood and Crocombe [8] who started initially from linear elastic analysis where a sandwich assembly was subjected to combined loading. They succeeded to establish closed-form equations for shear and peel stresses; those were assumed to be constant through the thickness of the joint. They improved their work and studied the nonlinearity of the adhesive using a hyperbolic tangent approximation, numerical results were obtained by using a finite-difference method. However, the hydrostatic stress tensor was disregarded for sake of simplicity [9]. In a separate work [10], the same authors extended the previous study for a full analysis to include also the non-linearity of the adherent. This latter work was also extended by Wang et al. [11] where the shear deformation in the substrates was considered in the adhesive failure study. They established a system of six first-order non-linear differential equations; those could be accurately solved by applying the finite difference method. Adams and Mallick [12] also reported the plastic behavior as either they applied successive loads until failure was reached or the full load was totally implemented. Thus they introduced a new method called linear effective modulus. In the same context, Adams et al. [13] tackled also the non-linear behavior of adhesive and adherents in a closed-form simple analytical model. However, it is applicable for non-yielding substrates with exclusively ductile adhesives and for yielding adherents or not with any type of adhesive. Tsai et al. [14] developed an improved version of the shear-lag model where the shear stress distribution along the adherent's thickness was considered to be linear; they concluded a closed-form analytical solution for the shear stress distribution for both SLJ and DLJ; the results brought were certainly more accurate than the classical shear-lag model. This latter approach was applied by Challita [15] to investigate the shear stress profile within a voided DLJ where a parametric study based on the void's size and position was included. Single-strap butt joint analytical investigation was the main concern of Li [16] who established closed-form solutions for both shear and peel stresses for both similar and dissimilar substrates. The model was validated by a 2D finite element simulation.

One may conclude from this brief historical overview that, despite the continuous improvement of the established models, all the aforementioned solutions have noticed the existence of the edge peak of stress without trying to reduce this effect, while in practical applications, the existence of such effect is the main reason of fracture of adhesively bonded assemblies.

Many authors have tried to reduce the stress concentrations at the joint's edges. One of the proposed solutions has been the use of spew fillet; however, the investigations of this aspect were limited to numerical and experimental efforts. Analytically, one can cite only the model of Frostig et al. [17] who applied a Closed-form High Order (CFHO) approach. The spew fillet was modeled as an equivalent tensile bar. Results have shown that increasing the spew fillet size leads to a decrement in the peak stress level at the edge.

The solution of variable thickness of the joint was developed analytically by Adams et al. [18]; they imposed a desired shear stress profile and searched for an adhesive thickness profile; they found a differential equation is solved for this variable thickness where thicker adhesive concentrate at the edges and thinner adhesive in the middle. Nevertheless, both proposed solutions seem very complex to be executed in practical joints since they suggest high geometric accuracy which is time-consuming in manufacturing and which increases the cost.

The mixed adhesive approach has imposed itself as one of the promising solutions to the edge effect problem. Raphael [19] was the first who put mixed adhesive joints under the spot: restraining this peak effect was achieved by implementing flexible low-modulus adhesive at these regions sustaining a huge strain while in the middle a stiff adhesive must be used to provide strength. da Silva [20] has detailed many aspects related to the mixed adhesive joints such as their importance in the transportation sector, manufacturing, design, strength approach, and practical applications. He mentioned two advantages of this technique: strength improvement and extension of the interval of operational temperatures. Similarly, Broughton and Fitton [21] have presented a full analysis of this mixed adhesive technique by showing first experimental strength improvement for metallic and composite mixed bonded specimens; then a numerical discussion on the influence of the adhesives Young's moduli and their lengths on the performance of the joint was presented. A pure experimental investigation on the shear strength of mixed adhesive metallic SLJ was carried out by da Silva and Lopes [22] where different types of adhesives were used; the joint's strength was predicted by a simple calculation. As a combination of experimental and numerical simulation of mixed adhesive joints, one may cite the works of Pires et al. [23] and Fitton and Broughton [24]: in both works, a parametric investigation has been carried out using Finite Element modeling under linear elastic behavior assumption. The influence of the adhesives Young's moduli and their lengths on shear and peel stresses was examined; this was accompanied by a couple of experimental tests on metallic SLJ specimens. However, all the cited works that are related to the mixed-adhesive technique are limited to either experimental or numerical analyses which do not offer general tendencies of behavior and are still dependent on the specific configuration of the assembly.

Purely analytical models tackling mixed adhesive joints aspect have been remarkably rare. Besides the work in [18], one should mention the model established by Srinivas [25] for both SLJ and DLJ cases. Nevertheless, the solution was calculated by numerical means. He concluded that assigning a short length of the overlap to the flexible adhesive and a longer length for the stiff one decreased the shear and peel stresses in both adhesives. In addition, increasing the length of the soft adhesive will increase stress concentration and thus the stiff adhesive must contribute more than the soft one in the overlap. Finally, the works of das Neves et al. [26], [27] have come to complete this short list of analytical models on mixed adhesive joints. This model was based on the work achieved in [17] for both SLJ and DLJ geometries and was validated numerically. They employed the established model to carry out a parametric study based mainly on the change of stiff and soft adhesive moduli, this was equivalent indeed to a temperature sweep. Both maximum shear and peel stresses were examined.

Besides the rare amount of works cited in the latter lines, there were no works tackling the aspect of mixed-adhesive joints from an analytical point of view; in addition, the improved-shear lag model [14] has never been applied and the influence of many geometric and mechanical parameters on the shear stress peaks has not been carried out in depth. The main purpose of this paper is to establish a closed-form analytical solution for the shear stress profile along a mixed adhesive DLJ length using the improved shear-lag model presented in [14], which considers a linear shear stress distribution through substrates' thickness. Then this model is to be validated using 2D FEM analysis on ABAQUS CAE software. Finally, a very detailed parametric study based on the change of the adhesives Young's moduli, lengths, and thicknesses will be performed to investigate the peak of shear stresses.

2. Analytical formulation
2.1 *Double lap geometry*

DLJ geometry is advantageous over SLJ due to the symmetry which reduces peel stresses exhibited by the bending moment of the non-symmetric geometry of SLJ.

In addition, this symmetry allows considering either the upper or the lower half only for numerical simulations. DLJ model as shown in Figure 1 consists of three adherents, two outers (cantilevered at the left) and one inner (subjected to a static axial force P_0 at the right) having a thickness twice of each of the outer substrates. They are assembled by two adhesive layers based on the mixed adhesive approach where the soft adhesive is applied at both joint ends (regions (1) & (3)) and stiff adhesive at the middle of the overlap (region (2)).
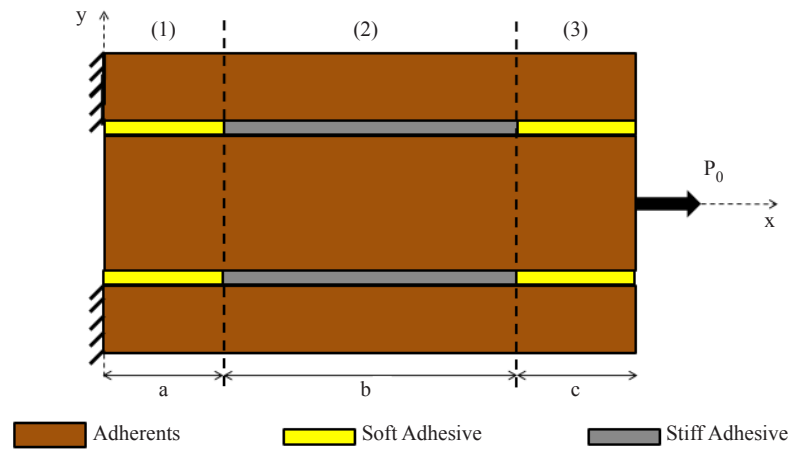
Figure 1. Double-lap joint assembly as used in this analysis

2.2 Improved shear-lag approach

The analytical model presented in this work is based on the improved shear-lag concept proposed in [14] for both SLJ and DLJ where the adherent shear stress distribution along the thickness is assumed to change linearly as illustrated in Figure 2, unlike other works where shear stress distribution was supposed to be constant. The shear stress along the adhesive thickness was assumed to be constant; the analysis has been conducted under the linear elastic behavior of materials where no plastic deformations were taken into consideration.

2.3 Equations
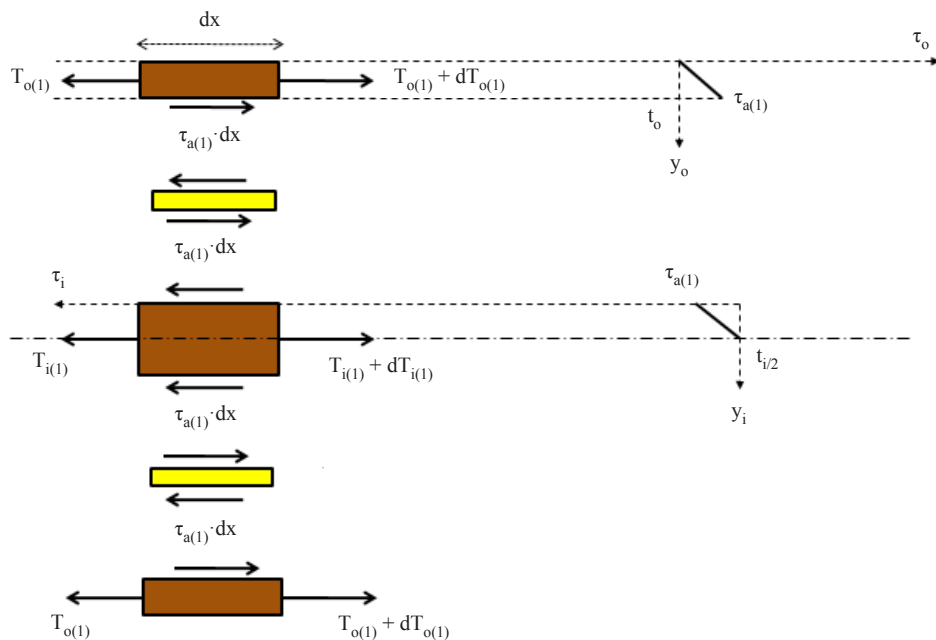
Figure 2. Free body diagram of differential elements of region (1)

The mathematical formulation is derived by applying Hooke's law, equilibrium equations, and the first linear regression of the adherent modified shear-lag on the differential elements (Figure 2). In this section, only equations of region (1) (0 < x < a) are shown. Those for regions (2) (a < x < a + b) and (3) (a + b < x < a + b + c) are obtained by changing the index from 1 to 2 and 3.

Due to the symmetry provided by the DLJ, the lower half part of the central substrate and the whole lower adherent with their corresponding adhesive bond line have been discarded during this analysis.

Transversal shear stress distribution of the upper (Eq. 1) and central (Eq. 2) adherents are written applying linear regression:

$$\tau_{o(1)}(x, y_o) = \frac{\tau_{a(1)}(x)}{t_o} \cdot y_o \tag{1}$$

$$\tau_{i(1)}(x, y_i) = \tau_{a(1)}(x) \cdot \left(1 - 2 \cdot \frac{y_i}{t_i}\right) \tag{2}$$

Applying static equilibrium on the differential elements of the upper (Eq. 3) and central (Eq. 4) adherents one gets:

$$\frac{dT_{o(1)}}{dx} + \tau_{a(1)} = 0 \tag{3}$$

$$\frac{dT_{i(1)}}{dx} - 2 \cdot \tau_{a(1)} = 0 \tag{4}$$

Applying Hooke's law on the substrates, one gets the shear strain equation for the upper adherent (Eq. 5) and central one (Eq. 6):

$$\gamma_{o(1)}(x, y_o) = \frac{\tau_{o(1)}(x, y_o)}{G_o} \tag{5}$$

$$\gamma_{i(1)}(x, y_i) = \frac{\tau_{i(1)}(x, y_i)}{G_i} \tag{6}$$

However, the latter equations can be written in their differential forms respectively, thus:

$$\gamma_{o(1)}(x, y_o) = \frac{\partial u_{o(1)}(x, y_o)}{\partial y_o} \tag{7}$$

$$\gamma_{i(1)}(x, y_i) = \frac{\partial u_{i(1)}(x, y_i)}{\partial y_i} \tag{8}$$

Axial displacement of the outer adherent is obtained by replacing equations (1) and (5) in (7) and integrating along its thickness:

$$u_{o(1)}(x, y_o) = u_{to(1)}(x) + \int_0^{y_o} \gamma_{o(1)}(x, y_o) \cdot dy_o = u_{to(1)}(x) + \frac{\tau_{a(1)}(x)}{2 \cdot G_o \cdot t_o} \cdot y_o^2$$

The displacement at the top surface of the upper substrate could be found in terms of the interfacial displacement $u_{io(1)}$ between the adhesive and the upper adherent; it is calculated by replacing y_o with t_o in $u_{o(1)}$:

$$u_{to(1)}(x) = u_{io(1)}(x) - \frac{\tau_{a(1)}(x) \cdot t_o}{2 \cdot G_o}$$

Hence the axial displacement of the outer adherent becomes:

$$u_{o(1)}(x, y_o) = u_{io(1)}(x) - \frac{\tau_{a(1)}(x) \cdot t_o}{2 \cdot G_o} + \frac{\tau_{a(1)}(x)}{2 \cdot G_o \cdot t_o} \cdot y_o^2 \tag{9}$$

Again the axial displacement of the inner adherent is expressed by substituting equations (2) and (6) in (8) and integrating along the thickness:

$$u_{i(1)}(x, y_i) = u_{ii(1)}(x) + \int_0^{y_i} \gamma_{i(1)}(x, y_i) \cdot dy_i$$

$$u_{i(1)}(x, y_i) = u_{ii(1)}(x) + \frac{\tau_{a(1)}(x)}{G_i} \left(y_i - \frac{y_i^2}{t_i} \right) \tag{10}$$

The next step consists in applying Hooke's law for axial stress as both adherents are subjected to a longitudinal force, obtaining equation (11) for the upper adherent and (12) for the central one:

$$\sigma_{o(1)}(x, y_o) = E_o \cdot \frac{\partial u_{o(1)}(x, y_o)}{\partial x} \tag{11}$$

$$\sigma_{i(1)}(x, y_i) = E_i \cdot \frac{\partial u_{i(1)}(x, y_i)}{\partial x} \tag{12}$$

Axial forces along the adherent's length are expressed per unit width of the upper adherent by combining equations (9) and (11):

$$T_{o(1)}(x) = \int_0^{t_o} \sigma_{o(1)}(x, y_o) \cdot dy_o$$

$$T_{o(1)}(x) = E_o \cdot t_o \cdot \left(\frac{du_{io(1)}(x)}{dx} - \frac{t_o}{3 \cdot G_o} \cdot \frac{d\tau_{a(1)}(x)}{dx} \right) \tag{13}$$

And for the central adherent, equation (10) is combined with equation (12):

$$T_{i(1)}(x) = 2 \cdot \int_0^{\frac{t_i}{2}} \sigma_{i(1)}(x, y_i) \cdot dy_i$$

$$T_{i(1)}(x) = E_i \cdot t_i \cdot \left(\frac{du_{ii(1)}(x)}{dx} + \frac{t_i}{6 \cdot G_i} \cdot \frac{d\tau_{a(1)}(x)}{dx} \right) \tag{14}$$

Applying now Hooke's law for the shear behavior of the adhesive leads to the following:

$$\tau_{a(1)}(x) = \frac{u_{ii(1)}(x) - u_{io(1)}(x)}{t_a} G_{a1} \tag{15}$$

Then, $\dfrac{du_{io(1)}(x)}{dx}$ and $\dfrac{du_{ii(1)}(x)}{dx}$ are respectively extracted from equations (13) and (14). Replacing those latter quantities in equation (15) after differentiating it with respect to x, gives:

$$\left(1 + \frac{G_{a1}}{t_a} \left(\frac{t_i}{6 \cdot G_i} + \frac{t_o}{3 \cdot G_o} \right) \right) \frac{d\tau_{a(1)}(x)}{dx} = \left(\frac{T_{i(1)}(x)}{E_i \cdot t_i} - \frac{T_{o(1)}(x)}{E_o \cdot t_o} \right) \frac{G_{a1}}{t_a}$$

Differentiating the previous equation with respect to x and then using equations (3) and (4) to replace $\dfrac{dT_{o(1)}}{dx}$ and $\dfrac{dT_{i(1)}}{dx}$, the purpose to establish an equation of $t_{a(1)}$ exclusively will be reached. This will provide a second-order differential equation:

$$\frac{d^2 \tau_{a(1)}(x)}{dx^2} - \beta_1^2 \cdot \tau_{a(1)}(x) = 0 \tag{16}$$

where:

$$\beta_1^2 = \frac{\dfrac{G_{a1}}{t_a} \left(\dfrac{2}{E_i \cdot t_i} + \dfrac{1}{E_o \cdot t_o} \right)}{\left[1 + \dfrac{G_{a1}}{t_a} \left(\dfrac{t_i}{6 \cdot G_i} + \dfrac{t_o}{3 \cdot G_o} \right) \right]}$$

Solving (16), gives the mathematical expression of the adhesive shear stress:

$$\tau_{a(1)}(x) = A_1 \sinh(\beta_1 \cdot x) + B_1 \cosh(\beta_1 \cdot x) \tag{17}$$

where A_1 and B_1 are two integration constants calculated by applying the appropriate boundary and continuity conditions.

However, boundary and continuity conditions apply to axial forces and axial displacements of the substrates; in other words, one must develop the expressions of the axial displacements relying on equations (9) and (10) and the axial forces relying on equations (13) and (14). Those are dependent on the adhesive shear stress and the displacements at the interfaces. Since the expression of the adhesive shear is already established in equation (17), the coming task consists in

determining the interfacial displacements and axial forces in the substrates.

Replacing equation (17) in (15) and inverting, the following equation (18) is obtained:

$$u_{ii(1)}(x) - u_{io(1)}(x) = \frac{t_a}{G_{a1}} \big(A_1 \sinh(\beta_1 \cdot x) + B_1 \cosh(\beta_1 \cdot x) \big) \tag{18}$$

Adding the expressions of $\dfrac{du_{io(1)}(x)}{dx}$ and $\dfrac{du_{ii(1)}(x)}{dx}$ member to member extracted from equations (13) and (14), one gets:

$$\frac{du_{ii(1)}(x)}{dx} + \frac{du_{io(1)}(x)}{dx} = \frac{T_{i(1)}(x)}{E_i \cdot t_i} - \frac{T_{o(1)}(x)}{E_o \cdot t_o} - \left(\frac{t_i}{6 \cdot G_i} - \frac{t_o}{3 \cdot G_o} \right) \frac{d\tau_{a(1)}(x)}{dx}$$

By differentiating again this latter equation along the variable x and then combining it with equations (3), (4), and (17), all the second members will be converted into an expression in terms of the variable x as follows:

$$\frac{d^2 \big(u_{ii(1)}(x) + u_{io(1)}(x) \big)}{dx^2} = \Gamma_1 \big(A_1 \sinh(\beta_1 \cdot x) + B_1 \cosh(\beta_1 \cdot x) \big)$$

where:

$$\Gamma_1 = \left(\frac{2}{E_i \cdot t_i} - \frac{1}{E_o \cdot t_o} \right) - \left(\frac{t_i}{6 \cdot G_i} - \frac{t_o}{3 \cdot G_o} \right) \cdot \beta_1^2$$

By integrating twice this latter equation along x, equation (19) is obtained where two additional integration constants, C_1 and D_1 will appear:

$$u_{ii(1)}(x) + u_{io(1)}(x) = \frac{\Gamma_1}{\beta_1^2} A_1 \sinh(\beta \cdot x) + \frac{\Gamma_1}{\beta_1^2} B_1 \cosh(\beta \cdot x) + C_1 \cdot x + D_1 \tag{19}$$

The two interfacial displacements in equations (18) and (19) are unknowns; since the system is linear, the interfacial displacement could be easily found:

$$u_{ii(1)}(x) = \frac{1}{2} \Big[\lambda_1^* A_1 \sinh(\beta_1 \cdot x) + \lambda_1^* B_1 \cosh(\beta_1 \cdot x) + C_1 \cdot x + D_1 \Big] \tag{20}$$

$$u_{io(1)}(x) = \frac{1}{2} \Big[\mu_1^* A_1 \sinh(\beta_1 \cdot x) + \mu_1^* B_1 \cosh(\beta_1 \cdot x) + C_1 \cdot x + D_1 \Big] \tag{21}$$

where:

$$\lambda_1^* = \frac{\Gamma_1}{\beta_1^2} + \frac{t_a}{G_{a1}}$$

$$\mu_1^* = \frac{\Gamma_1}{\beta_1^2} - \frac{t_a}{G_{a1}}$$

To keep x as the lone variable in the displacement of the adherent, one calculates the average axial displacement through the thickness of the outer adherent by applying the following equation:

$$\left\langle u_{o(1)} \right\rangle (x) = \frac{1}{t_o} \int_0^{t_o} u_{o(1)}(x, y_o) \cdot dy_o$$

Replacing equation (9) in the previous integral, one gets equation (22):

$$\left\langle u_{o(1)} \right\rangle (x) = u_{io(1)}(x) - \frac{\tau_{a(1)}(x) \cdot t_o}{3 \cdot G_o} \qquad (22)$$

Repeating the calculation of the average displacement for the inner substrate and then replacing equation (10) in the integral, one gets equation (23):

$$\left\langle u_{i(1)} \right\rangle (x) = \frac{2}{t_i} \int_0^{t_i/2} u_{i(1)}(x, y_i) \cdot dy_i$$

$$\left\langle u_{i(1)} \right\rangle (x) = u_{ii(1)}(x) + \frac{\tau_{a(1)}(x) \cdot t_i}{6 \cdot G_i} \qquad (23)$$

Combining equations (17) and (21) with (22) on one side, and (17) and (20) with (23) on the other side, the final expressions of the average axial displacements, numbered by equations (24) and (25) are determined as follows:

$$\left\langle u_{o(1)} \right\rangle (x) = \frac{1}{2} \left[\mu_1 A_1 \sinh(\beta_1 \cdot x) + \mu_1 B_1 \cosh(\beta_1 \cdot x) + C_1 \cdot x + D_1 \right] \qquad (24)$$

$$\left\langle u_{i(1)} \right\rangle (x) = \frac{1}{2} \left[\lambda_1 A_1 \sinh(\beta_1 \cdot x) + \lambda_1 B_1 \cosh(\beta_1 \cdot x) + C_1 \cdot x + D_1 \right] \qquad (25)$$

where:

$$\mu_1 = \mu_1^* - \frac{2 \cdot t_o}{3 \cdot G_o}$$

$$\lambda_1 = \lambda_1^* + \frac{t_i}{3 \cdot G_i}$$

Combining equations (17) and (21) with (13) on one side, and (17) and (20) with (14) on the other side, the final expressions of the axial forces per unit width, numbered by (26) and (27) are determined as follows:

$$T_{o(1)}(x) = \frac{E_o \cdot t_o}{2} \left[\beta_1 \mu_1 A_1 \cosh(\beta_1 \cdot x) + \beta_1 \mu_1 B_1 \sinh(\beta_1 \cdot x) + C_1 \right] \tag{26}$$

$$T_{i(1)}(x) = \frac{E_i \cdot t_i}{2} \left[\beta_1 \lambda_1 A_1 \cosh(\beta_1 \cdot x) + \beta_1 \lambda_1 B_1 \sinh(\beta_1 \cdot x) + C_1 \right] \tag{27}$$

As stated earlier, since the free body diagrams in regions (2) and (3) are identical to the one in region (1) as a sketch but in different amounts, one can take inspiration from the expressions established for region (1) by changing the appropriate indexes as follows:

Region 2: a < x < a + b

$$\tau_{a(2)}(x) = A_2 \sinh(\beta_2 \cdot x) + B_2 \cosh(\beta_2 \cdot x) \tag{28}$$

$$\langle u_{o(2)} \rangle(x) = \frac{1}{2} \left[\mu_2 A_2 \sinh(\beta_2 \cdot x) + \mu_2 B_2 \cosh(\beta_2 \cdot x) + C_2 \cdot x + D_2 \right] \tag{29}$$

$$\langle u_{i(2)} \rangle(x) = \frac{1}{2} \left[\lambda_2 A_2 \sinh(\beta_2 \cdot x) + \lambda_2 B_2 \cosh(\beta_2 \cdot x) + C_2 \cdot x + D_2 \right] \tag{30}$$

$$T_{o(2)}(x) = \frac{E_o \cdot t_o}{2} \left[\beta_2 \mu_2 A_2 \cosh(\beta_2 \cdot x) + \beta_2 \mu_2 B_2 \sinh(\beta_2 \cdot x) + C_2 \right] \tag{31}$$

$$T_{i(2)}(x) = \frac{E_i \cdot t_i}{2} \left[\beta_2 \lambda_2 A_2 \cosh(\beta_2 \cdot x) + \beta_2 \lambda_2 B_2 \sinh(\beta_2 \cdot x) + C_2 \right] \tag{32}$$

It should be noticed that b_2, m_2, and l_2 have the same expressions as b_1, m_1, and l_1 respectively, by replacing exclusively G_{a1} with G_{a2}.

Region 3: a + b < x < a + b + c

$$\tau_{a(3)}(x) = A_3 \sinh(\beta_3 \cdot x) + B_3 \cosh(\beta_3 \cdot x) \tag{33}$$

$$\langle u_{o(3)} \rangle(x) = \frac{1}{2} \left[\mu_3 A_3 \sinh(\beta_3 \cdot x) + \mu_3 B_3 \cosh(\beta_3 \cdot x) + C_3 \cdot x + D_3 \right] \tag{34}$$

$$\langle u_{i(3)} \rangle(x) = \frac{1}{2} \left[\lambda_3 A_3 \sinh(\beta_3 \cdot x) + \lambda_3 B_3 \cosh(\beta_3 \cdot x) + C_3 \cdot x + D_3 \right] \tag{35}$$

$$T_{o(3)}(x) = \frac{E_o \cdot t_o}{2} \left[\beta_3 \mu_3 A_3 \cosh(\beta_3 \cdot x) + \beta_3 \mu_3 B_3 \sinh(\beta_3 \cdot x) + C_3 \right] \tag{36}$$

$$T_{i(3)}(x) = \frac{E_i \cdot t_i}{2} \left[\beta_3 \lambda_3 A_3 \cosh(\beta_3 \cdot x) + \beta_3 \lambda_3 B_3 \sinh(\beta_3 \cdot x) + C_3 \right] \tag{37}$$

It should be noticed that b_3, m_3, and l_3 have the same expressions as b_1, m_1, and l_1 respectively, by replacing

exclusively G_{a1} with G_{a3}.

To find the three expressions of the adhesive shear stresses, one must calculate A_1, B_1, A_2, B_2, A_3, and B_3 according to equations (17), (28), and (33). This calculation relies on continuity and boundary conditions of the axial displacements and forces applied at both ends of the overlap and at the interface of two adjacent regions.

The mathematical expressions of these equations are listed as follows:

(C1) $\left\langle u_{o(1)} \right\rangle(0) = 0$

(C2) $T_{i(1)}(0) = 0$

(C3) $T_{o(1)}(a) = T_{o(2)}(a)$

(C4) $\left\langle u_{o(1)} \right\rangle(a) = \left\langle u_{o(2)} \right\rangle(a)$

(C5) $T_{i(1)}(a) = T_{i(2)}(a)$

(C6) $\left\langle u_{i(1)} \right\rangle(a) = \left\langle u_{i(2)} \right\rangle(a)$

(C7) $T_{o(2)}(a+b) = T_{o(3)}(a+b)$

(C8) $\left\langle u_{o(2)} \right\rangle(a+b) = \left\langle u_{o(3)} \right\rangle(a+b)$

(C9) $T_{i(2)}(a+b) = T_{i(3)}(a+b)$

(C10) $\left\langle u_{i(2)} \right\rangle(a+b) = \left\langle u_{i(3)} \right\rangle(a+b)$

(C11) $T_{o(3)}(a+b+c) = 0$

(C12) $T_{i(3)}(a+b+c) = P_0$

By expanding and arranging the equation delivered from each condition, a symbolic linear system of 12 equations with 12 unknowns will be generated. The constants that are multiplying the unknowns are complicated. For the sake of clarity and simplicity, each group of constants was unified by a single constant such as:

$$K_1 = \cosh(\beta_1 \cdot a)$$

$$K_2 = \cosh(\beta_2 \cdot a)$$

$$K_3 = \cosh(\beta_2 \cdot (a+b))$$

$$K_4 = \cosh(\beta_3 \cdot (a+b))$$

$$K_5 = \cosh(\beta_3 \cdot (a+b+c))$$

$$S_1 = \sinh(\beta_1 \cdot a)$$

$$S_2 = \sinh(\beta_2 \cdot a)$$

$$S_3 = \sinh(\beta_2 \cdot (a+b))$$

$$S_4 = \sinh(\beta_3 \cdot (a+b))$$

$$S_5 = \sinh(\beta_3 \cdot (a+b+c))$$

The matrix form of the 12-equations-system is:

$$[k] \cdot X = P \tag{38}$$

Where:

$$[k] = \begin{bmatrix}
0 & \mu_1 & 0 & 1 & 0 & 0 & 0 & 0 & 0 & 0 & 0 & 0 \\
\beta_1 \cdot \lambda_1 & 0 & 1 & 0 & 0 & 0 & 0 & 0 & 0 & 0 & 0 & 0 \\
\beta_1 \cdot \mu_1 \cdot K_1 & \beta_1 \cdot \mu_1 \cdot S_1 & 1 & 0 & -\beta_2 \cdot \mu_2 \cdot K_2 & -\beta_2 \cdot \mu_2 \cdot S_2 & -1 & 0 & 0 & 0 & 0 & 0 \\
\mu_1 \cdot S_1 & \mu_1 \cdot K_1 & a & 1 & -\mu_2 \cdot S_2 & -\mu_2 \cdot K_2 & -a & -1 & 0 & 0 & 0 & 0 \\
\beta_1 \cdot \lambda_1 \cdot K_1 & \beta_1 \cdot \lambda_1 \cdot S_1 & 1 & 0 & -\beta_2 \cdot \lambda_2 \cdot K_2 & -\beta_2 \cdot \lambda_2 \cdot S_2 & -1 & 0 & 0 & 0 & 0 & 0 \\
\lambda_1 \cdot S_1 & \lambda_1 \cdot K_1 & a & 1 & -\lambda_2 \cdot S_2 & -\lambda_2 \cdot K_2 & -a & -1 & 0 & 0 & 0 & 0 \\
0 & 0 & 0 & 0 & \beta_2 \cdot \mu_2 \cdot K_3 & \beta_2 \cdot \mu_2 \cdot S_3 & 1 & 0 & -\beta_3 \cdot \mu_3 \cdot K_4 & -\beta_3 \cdot \mu_3 \cdot S_4 & -1 & 0 \\
0 & 0 & 0 & 0 & \mu_2 \cdot S_3 & \mu_2 \cdot K_3 & (a+b) & 1 & -\mu_3 \cdot S_4 & -\mu_3 \cdot SK_4 & -(a+b) & -1 \\
0 & 0 & 0 & 0 & \beta_2 \cdot \lambda_2 \cdot K_3 & \beta_2 \cdot \lambda_2 \cdot S_3 & 1 & 0 & -\beta_3 \cdot \lambda_3 \cdot K_4 & -\beta_3 \cdot \lambda_3 \cdot S_4 & -1 & 0 \\
0 & 0 & 0 & 0 & \lambda_2 \cdot S_3 & \lambda_2 \cdot K_3 & (a+b) & 1 & -\lambda_3 \cdot S_4 & -\lambda_3 \cdot K_4 & -(a+b) & -1 \\
0 & 0 & 0 & 0 & 0 & 0 & 0 & 0 & \beta_3 \cdot \mu_3 \cdot K_5 & \beta_3 \cdot \mu_3 \cdot S_5 & 1 & 0 \\
0 & 0 & 0 & 0 & 0 & 0 & 0 & 0 & \beta_3 \cdot \lambda_3 \cdot K_5 & \beta_3 \cdot \lambda_3 \cdot K_5 & 1 & 0
\end{bmatrix}$$

$$X = \begin{bmatrix} A_1 \\ B_1 \\ C_1 \\ D_1 \\ A_2 \\ B_2 \\ C_2 \\ D_2 \\ A_3 \\ B_3 \\ C_3 \\ D_3 \end{bmatrix} \quad \text{and} \quad P = \begin{bmatrix} 0 \\ 0 \\ 0 \\ 0 \\ 0 \\ 0 \\ 0 \\ 0 \\ 0 \\ 0 \\ 0 \\ \dfrac{2P_0}{E_i t_i} \end{bmatrix}$$

Applying the symbolic solver module in MATLAB, the unknown vector X, and thus the integration constants could be calculated by inverting equation (38):

$$X = [k]^{-1} \cdot P \tag{39}$$

3. Numerical validation

Numerical simulation is the tool adopted in this study to validate the analytical expression of the adhesive shear stress established in the previous section. This has been executed through a 2D finite element analysis using the

commercial software ABAQUS CAE. As stated earlier, due to the symmetry of the DLJ only the upper half of the joint has been simulated under appropriate boundary conditions.

3.1 *Parameters*

The geometrical and mechanical parameters used for this model have been inspired by previous work [21] on mixed adhesive joints. They are summarized in Table 1.

Table 1. Parameters of the 2D FEA

Parameter	Symbol	Value
Region (1) soft adhesive length	a	10 mm
Region (2) stiff adhesive length	b	30 mm
Region (3) soft adhesive length	c	10 mm
Thickness of the outer adherent	t_o	1.4 mm
Length of outer adherent	L_o	50 mm
Young's modulus of the outer adherent	E_o	169 GPa
Thickness of the inner adherent	t_i	2.8 mm
Length of inner adherent	L_i	50 mm
Young's modulus of the inner adherent	E_i	169 GPa
Poisson ratio of the adherents	$v_{o,i}$	0.3
Thickness of the adhesive bondline	t_a	0.25 mm
Young's modulus of the adhesive (1)	E_{a1}	0.37 GPa
Young's modulus of the adhesive (2)	E_{a2}	2.7 GPa
Young's modulus of the adhesive (3)	E_{a3}	0.37 GPa
Poisson ratio of adhesives (1), (2), & (3)	v_a	0.34
Axial static pressure per unit width	P_0	1,000 N/mm

3.2 *Modeling*

The model consists of three isotropic parts: adherent plates, and soft and stiff adhesives having the geometrical and mechanical properties listed in Table 1.

The overlap is meshed using CPE4R element type as described in Figure 3 where its length is divided into 225 elements (45 elements per 10 mm) with a double bias toward the edges in each region, 15 elements single bias towards the adhesive interface for the thickness of adherents. This configuration was derived from the numerical work in [23]. Concerning the adhesive bond line thickness meshing, a convergence study has been performed to adopt the

suitable choice. The starting trial was consisting of 6 elements where the shear stress profile through the joint length was measured. Then the number of elements was increased to 12; the relative difference of the results (i.e., shear stress profile) with respect to the previous trial was found to be 1.87%. In the third trial, the number of elements was incremented to 15 which gave a relative difference with respect to the preceding trial (i.e., 12 elements) 0.24%. This iterative process has continued until the relative difference has relatively stabilized and at a low percentage. In addition, for each trial, the calculation time was also reported. All this study is summarized in Table 2. Referring to this latter table, 30 elements were adopted to plot the final shear stress distribution profile along the overlap as it accords between results accuracy and time required to realize the calculations.

Table 2. Convergence study of adhesive meshing along its thickness

Adhesive thickness elements' number	Max. error of two consecutive mesh (%)	Time of calculation (s)
6	Control mesh	171
12	1.87	191
20	0.24	218
30	0.065	252
40	0.021	286

As mentioned in Section 2.1, only the upper half of the structure has been analyzed. The left side of the upper adherent is cantilevered while the bottom line of the central adherent (line of symmetry) is blocked from transverse displacement in pursuit to simulate the whole DLJ with minimum exertion and complexity. The external axial load of 1,000 N/mm has been implemented in the software in terms of pressure applied at the right end of the central substrate.
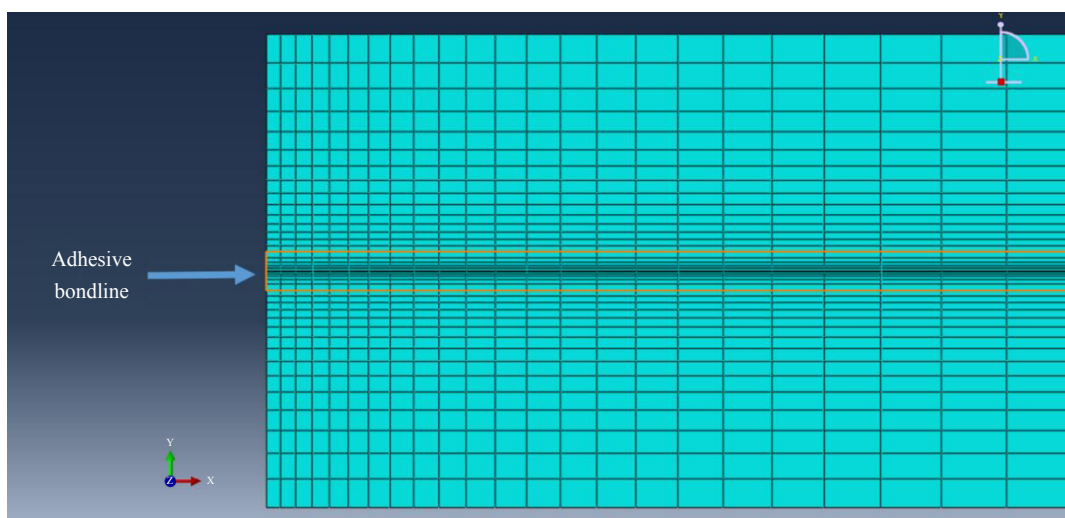
Figure 3. Overlap meshing illustration

3.3 Results

According to the error percentage calculated between both analytical and numerical values as illustrated in Figure 4, it is obvious that the highest deviation (3-3.9% error) between both models shows the lowest contribution (0.48%) throughout the joint; while the greatest convergence (< 1% error), exhibits the highest occurrence (52.41%).
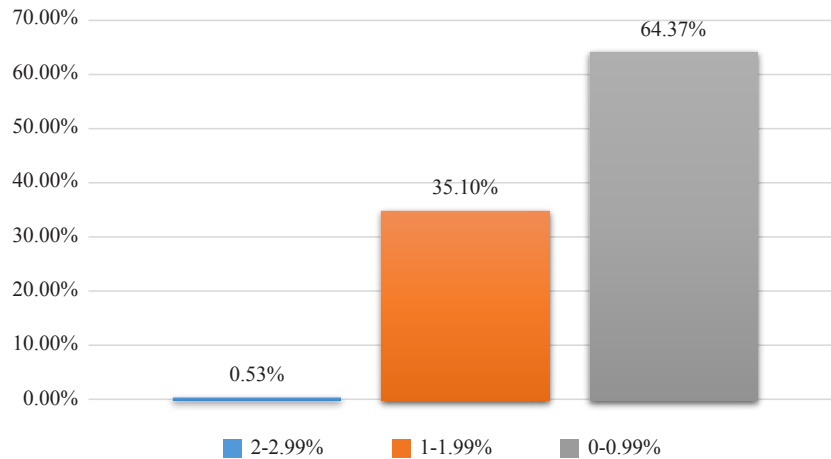

Figure 4. Distribution of calculated percent error values along the joint overlap

Consequently, the inaccuracy at the shear peaks which form the most critical part of the joint and where this work is almost all based, does not exceed 2.1%. Thus one can state that the proposed analytical model fits with high accuracy the numerical one with a maximum error of 3.9%. Figure 5 shows the coincidence of the two shear stress profiles.
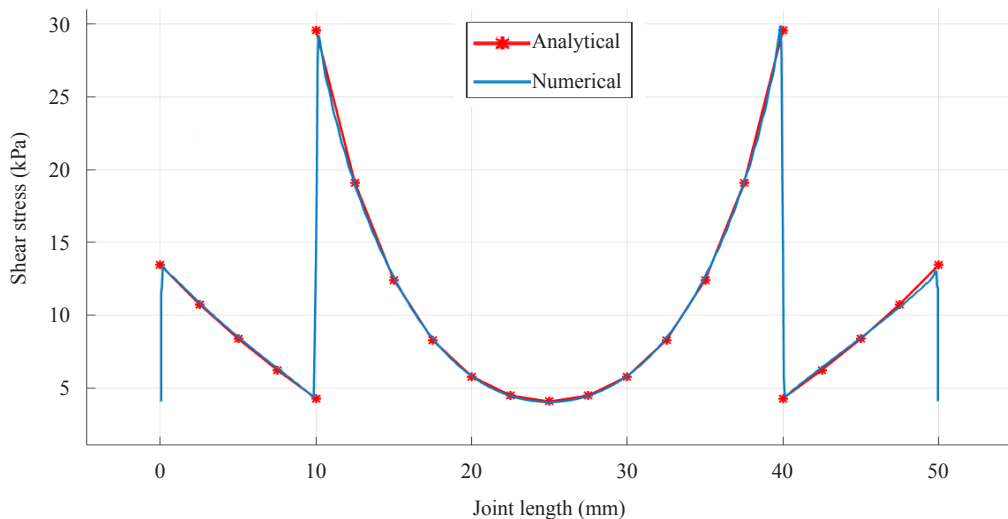
Figure 5. Analytical and numerical adhesive shear stress curves

In addition, Table 3 identifies the respective intervals of validity of the established analytical model related to the three studied parameters respecting the model of [24]. The table displays also the maximum error manifested between

the analytical and numerical profiles. Therefore, the analytical model is applicable for E_{a1}/E_{a2} ranging from 0.0037 to 0.74 that is E_1 can be any value between 0.01 and 2 GPa respectively. The same applies for a/b varying from 0 to infinity where the overlap can be modified between totally stiff to totally soft. Concerning the adhesive thickness, the analytical model is able to accurately estimate the shear stress distribution as it does not go below 40 μm and above 1,000 μm.

Table 3. Analytical model validation range regarding [24] model

Parameter	Value	Max. Error
t_a	40 μm	6%
	1,000 μm	7%
E_{a1}/E_{a2}	0.0037	9%
	0.74	13%
a/b	0	15.8%
	Inf	5.7%

4. Parametric investigation-discussion

The validated analytical model will be employed to carry out a detailed parametric investigation where the influence on the maximum shear stress developed in the joint's length will be put under the spot. Besides the reference model of [24] described in Table 1 where the substrates thickness configuration was 1.4-2.8-1.4, six additional configurations will be considered to examine the effect of the adherents' thicknesses, and those are: 1-2-1, 2-4-2, 2.5-5-2.5, 3-6-3, 3.5-7-3.5, and 4-8-4. For each of those latter configurations, three main parameters will be changed: the adhesives Young's moduli ratio E_{a1}/E_{a2} (Table 3), their lengths ratio a/b, and the adhesive layer thickness. It should be noticed that, in order to avoid the coupling effect, only one parameter will be changed per case, while all the remaining parameters keep their values as set in Table 1. Moreover, the soft adhesive lengths are kept all the time equal (a = c). Finally, all shear stress values along the adhesive length have been normalized with respect to the average shear stress in the joint; this was also adopted in [24].

4.1 *Adhesives young's moduli*

Similarly to what has been done in [23], [24], [27], the variation of the ratio E_{a1}/E_{a2} is based on keeping E_{a2} constant (2.7 GPa in that case) and changing E_{a1} to reach the desired ratio value. Those latter have been inspired by [23], [24] and summarized in Table 4 below.

It should be reminded that the ratio a/b and the adhesive thickness are kept unchanged in this sub-section, and are equal to 1/3 and 250 mm respectively.

The normalized shear stress profiles along the length of the joint 1.4-2.8-1.4 for most of the moduli ratios (and not all values to avoid non-clarity of superimposed curves) are plotted in the graph of Figure 6. The maximum shear stress in the stiff adhesive region decreases when E_{a1}/E_{a2} increases while the inverse is observed for the soft adhesive region. This means that, at a certain particular modulus ratio, the maximum stress in both regions is equal, this is known as the transition ratio. According to [20], the MADLJ is stronger than a pure adhesive joint when the stress level in the stiff region is higher than in the soft one, and thus useful values of E_{a1}/E_{a2} must remain below the transition ratio.

Table 4. List of Young's modulus used in the parametric study

| E_{a1} (GPa)	ν_{a1}	E_{a1}/E_{a2}
0.1	0.34	0.037
0.27	0.34	0.1
0.37	0.34	0.137
0.6	0.34	0.222
0.75	0.34	0.278
1	0.34	0.37
1.2	0.34	0.444
1.5	0.34	0.555
1.8	0.34	0.667

Moreover, in Figure 6, the normalized stress profile of a joint made from a pure stiff adhesive (E_{a1}/E_{a2} = 1) is shown. In the range of values considered in Table 4, the highest stress level in the MADLJ (E_{a1}/E_{a2} = 0.037; S_{max} = 3.97) remains less than the maximum stress for a pure stiff joint where S_{max} = 4.448. When E_{a1}/E_{a2} continues to decrease downwards to the lowest level, S_{max} in the MADLJ continues to increase until reaching the S_{max} of a pure stiff joint. This ratio of E_{a1}/E_{a2} is called the minimum ratio. Below this minimum, the maximum stress developed in the MADLJ exceeds the maximum stress in a pure stiff joint; consequently, the MADLJ technique is not advantageous anymore below this minimum ratio. All in all, the MADLJ technique is exclusively proper useful when the ratio E_{a1}/E_{a2} is between the interval [$E_{a1}/E_{a2})_{min}$; $E_{a1}/E_{a2})_{tr}$]. Those two boundaries of the interval change upon the geometrical parameters of the DLJ, this will be discussed sooner in this paper.

This aspect could be also illustrated in the graph of Figure 7 showing the variation of the maximum normalized shear stress as a function of E_{a1}/E_{a2} for pure soft joint, pure stiff joint, and mixed adhesive joint.

A similar graph was established in [27] for temperature-sensitive MADLJ. The maximum stress in the MADLJ is a compound curve (split at the transition ratio) where the first portion shows that the maximum stress occurs in the stiff region while this maximum takes place in the soft region (useless practically) in the second portion. Those two sub-curves intersect at the transition point, which for 1.4-2.8-1.4 configuration, measures about $E_{a1}/E_{a2})_{tr}$ = 0.265, generating S_{max_tr} = 2.164 (Figure 7(a)). On another side, $E_{a1}/E_{a2})_{min}$ represents the intersection between the MADLJ stress curve and the pure stiff joint curve (horizontal line S_{max} = 4.448). Since the range adopted in [24] does not go below 0.037, the intersection representing the minimum moduli ratio could not be detected on the graph. Further calculations for lower ratios using the validated analytical model have given $E_{a1}/E_{a2})_{min}$ = 0.0039 hence the useful ratio for this configuration (Figure 7(a)) is [0.0039; 0.265] where the maximum normalized stress decreases from S_{max_upper} = 4.448 to S_{max_tr} = 2.164. Practically, this means that the soft adhesive Young's modulus should belong to [0.0105; 0.716] GPa. One can remark that the lower boundary shows a very small value hence practically the options for selection are quite open. Figure 7(b) serves at visualizing graphically $E_{a1}/E_{a2})_{min}$ for the configuration 4-8-4, since this value exists in the considered range of the tested moduli ratios (Table 4) displayed in [24].
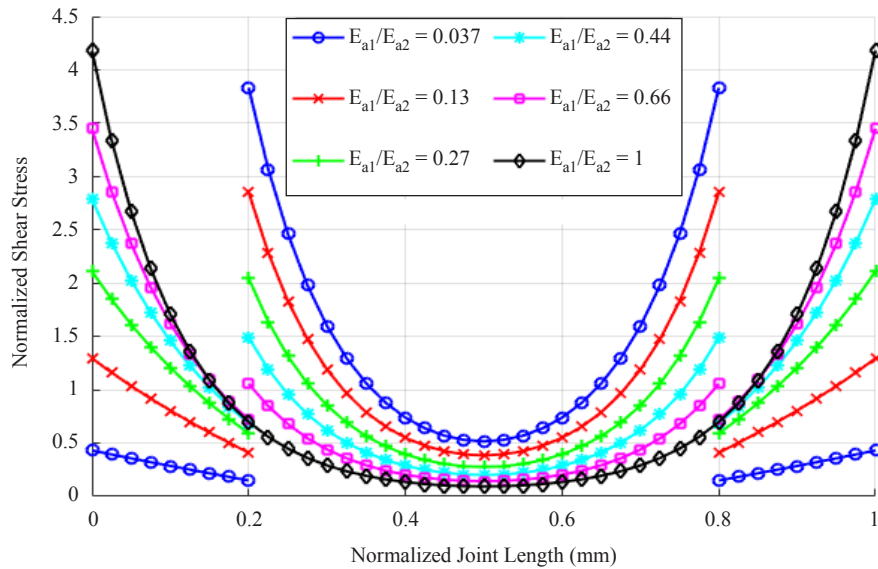
Figure 6. Evolution of normalized shear stress profile along the joint length for different ratios E_{a1}/E_{a2} for 1.4-2.8-1.4 configuration
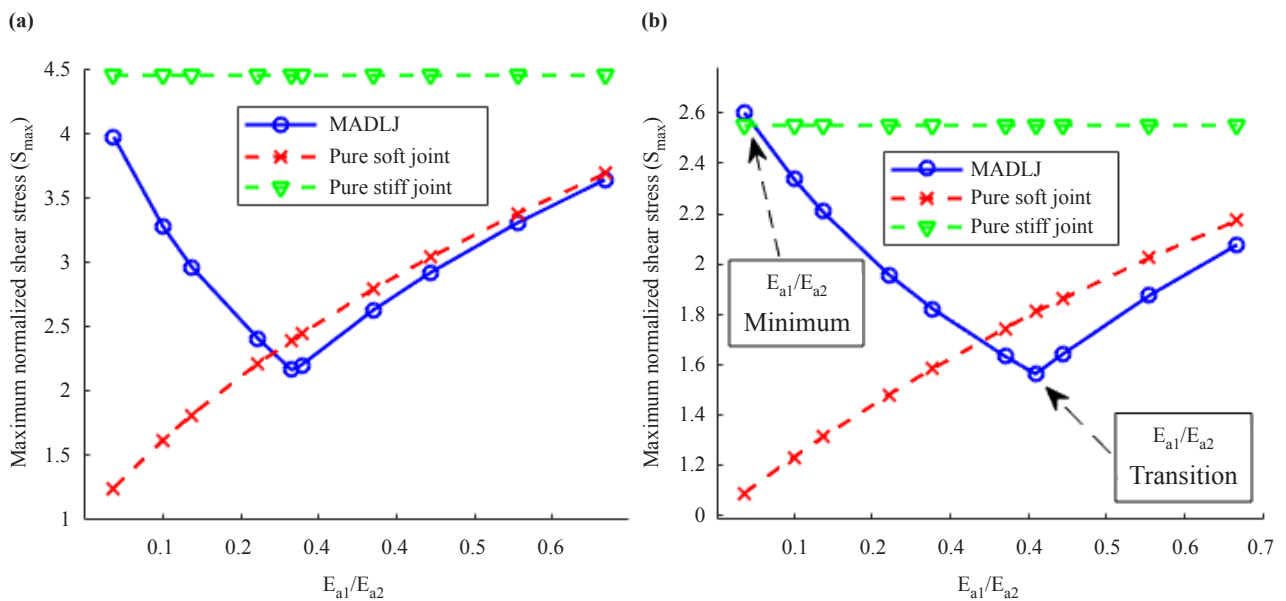
Figure 7. Evolution of the maximum normalized shear stress in terms of E_{a1}/E_{a2} in MADLJ, pure stiff and soft joints for (a) 1.4-2.8-1.4 and (b) 4-8-4 configurations

By extending this study to all the other configurations, results can be summarized in Table 5 below.

By observing the values in Table 5, one can deduce that both $E_{a1}/E_{a2})_{min}$ and $E_{a1}/E_{a2})_{tr}$ increase as the thickness of the substrate increases while the maximum stress level at the transition point decreases when the substrate's thickness increases. Increasing the structure's thickness from 1-2-1 to 4-8-4, the transition ratio increases by 79% while the maximum stress level decreases by 35%. The minimum modulus ratio on the other hand increases by 28% along with a 52% decrease in the stress level.

Table 5. Young's modulus transition and minimum ratios for different adherents' thicknesses

Configuration	1-2-1	1.4-2.8-1.4	2-4-2	2.5-5-2.5	3-6-3	3.5-7-3.5	4-8-4
$E_{a1}/E_{a2})_{tr}$	0.228	0.265	0.31	0.34	0.366	0.388	0.409
S_{max_tr}	2.403	2.164	1.936	1.805	1.706	1.625	1.564
$E_{a1}/E_{a2})_{min}$	0.0017	0.0039	0.0094	0.0167	0.0257	0.037	0.048
S_{max_upper}	5.293	4.448	3.69	3.278	2.974	2.739	2.551

Not only does S_{max_tr} decrease with the substrate's thickness increment, but also all stress levels at all the other E_{a1}/E_{a2} values lie within the useful interval as shown in the graph of Figure 8. At low ratio values, the stress levels are "discernible" showing clear differences where the stress order is inverse to the thickness ordered. As E_{a1}/E_{a2} increases, the stress levels in all thicknesses decrease and the curves look like to "converge" to very close values. Moreover, the slope of the curves decreases with the increment of the thickness of the adherent, and thus the margin of variabilities of maximum stress levels within the useful intervals of the moduli ratio is reduced. For instance, for 1-2-1 configuration, the maximum normalized stress interval is [2.403, 5.293] while for 4-8-4 this interval becomes [1.564, 2.602].
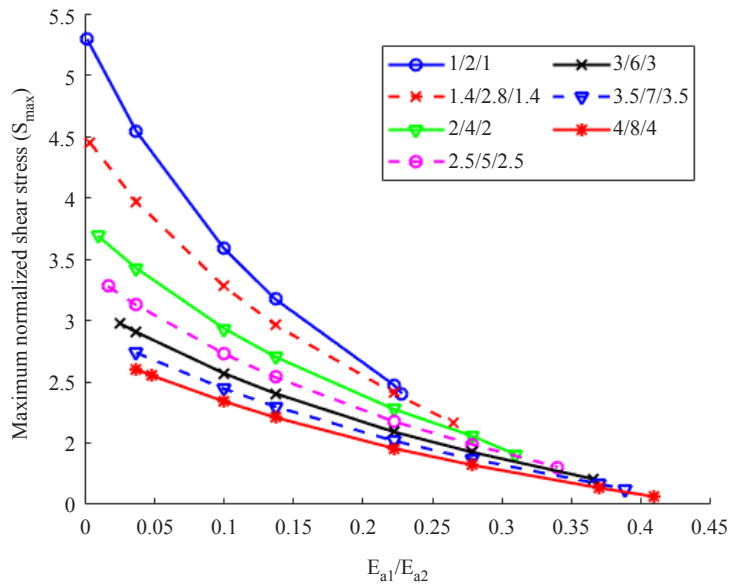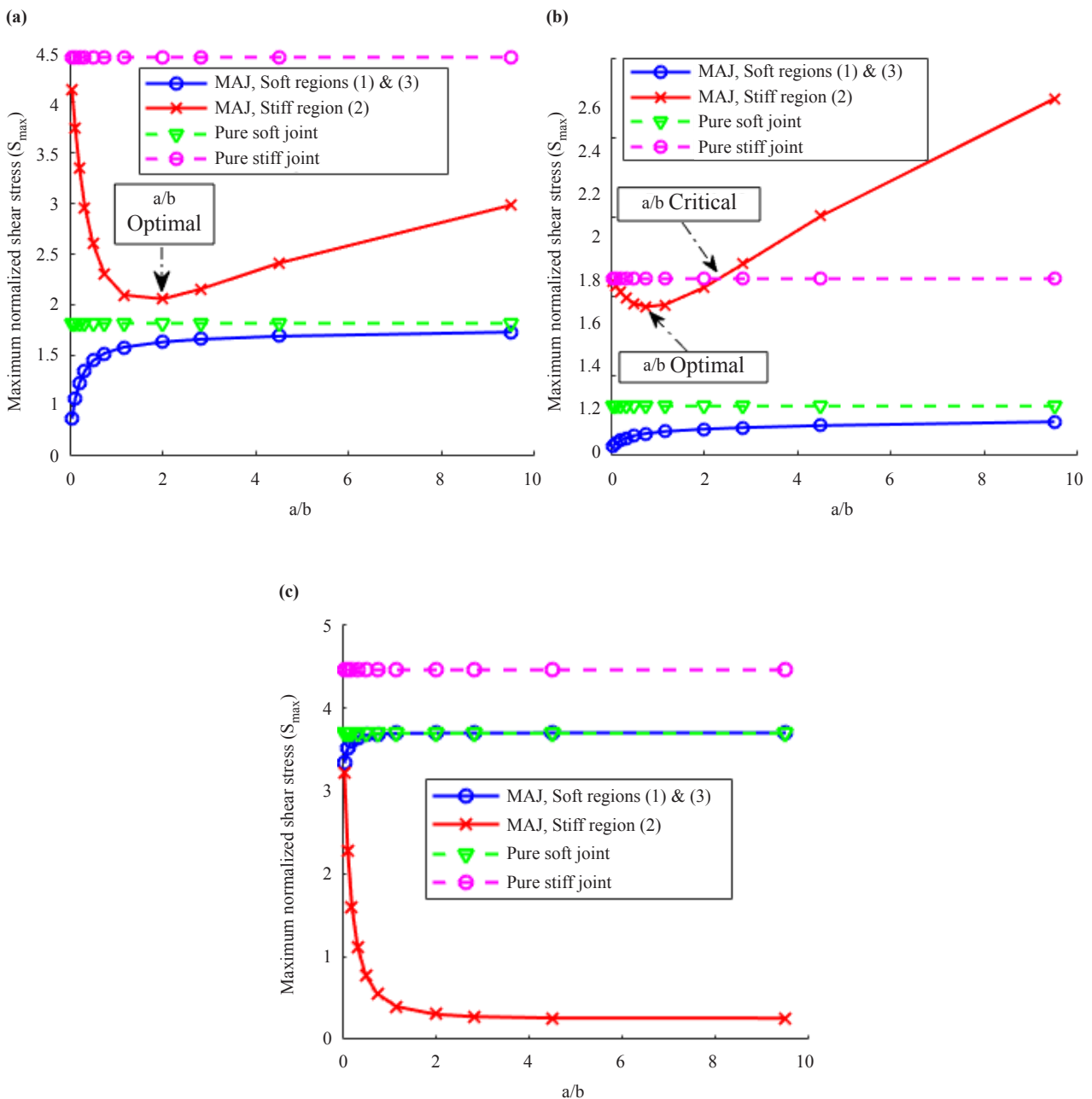

Figure 8. Evolution of the maximum normalized shear stress in the useful moduli ratio range for each adherent thickness

It should be noticed that the shear stress distribution could be affected by the values of E_{a1} or E_{a2} besides their ratio. A series of stiff and soft Young's moduli values was tested through the analytical model keeping the ratio all the time equal to 0.137. The analytical model displayed different shear stress profiles which fall in the validity range.

4.2 Adhesives lengths

Referring again to Table 1, E_{a1}/E_{a2} is kept constant at equal to 0.137 while the adhesive thickness remains equal to 250 mm as in [24]. In that original model, the ratio a/b was equal to 1/3. Figure 9(a) shows the variation of the maximum normalized shear stress S_{max} in the stiff and the soft adhesives for a 1.4-2.8-1.4 MADLJ for many values of the ratio a/b: 0.05, 0.12, 0.21, 0.33, 0.5, 0.75, 1.16, 2, 2.83, 4.5, and 9.5. It is obvious that a ratio a/b = 0 means practically a pure stiff joint, while a/b = means a pure soft joint.

Figure 9. Evolution of the maximum normalized shear stress in terms of a/b in MADLJ, pure stiff and soft joints for 1.4-2.8-1.4 configuration for (a) $E_{a1}/E_{a2} = 0.137$, (b) $E_{a1}/E_{a2} = 0.037$ and (c) $E_{a1}/E_{a2} = 0.667$

In Figure 9(a), one can remark that the maximum stress level in the stiff region passes through a minimum at a/b = 2 while the same parameter in the soft region increases monotonically but with lower slopes as the ratio a/b increases; it converges at S_{max} = 1.816 corresponding to the maximum normalized stress in a pure soft joint. It should be noticed that for all a/b ratios, the maximum stress level in the MADLJ remains lower than the maximum level recorded in a pure stiff joint. However, by selecting a lower E_{a1}/E_{a2} value, 0.037 (Figure 9(b)) but belonging to the useful range discussed earlier, one remark that the level of maximum stress increases in the stiff region and decreases in the soft region, but the curves tendencies are similar to those issued from the ratio of 0.137 (Figure 9(a)). In that case, the gap between the maximum stress level in a pure soft joint (S_{max}= 1.25) and the one in the soft region of the MADLJ increases, while, on the other hand, the corresponding curves for the stiff region intersect, as shown in Figure 9(b), defining a critical value of a/b, above which the pure stiff joint becomes more advantageous over MADLJ; this value is about 2.3; in addition, one remarks that, with the decrement of E_{a1}/E_{a2}, the optimal value of a/b generating the lowest S_{max} decreases, being about 0.75.

On another hand, by checking a higher value of E_{a1}/E_{a2}, out of the useful range, one observes a different trend of S_{max} in the MADLJ. Figure 9(c) shows this distribution for E_{a1}/E_{a2} = 0.667; in that case, S_{max} in the stiff region decreases sharply for low a/b values, then the amount of decrement occurs at very low slopes as a/b increases; while the inverse occurs in the soft region; the maximum normalized stress converges to S_{max} occurring in the pure soft joint (here it is 3.69). It is obvious that, outside the useful range, S_{max} in the soft region is higher than S_{max} in the stiff region. It should be noticed, that similar tendencies of the evolution of the maximum shear stress in the MADLJ for different values of E_{a1}/E_{a2} were also observed in [27].
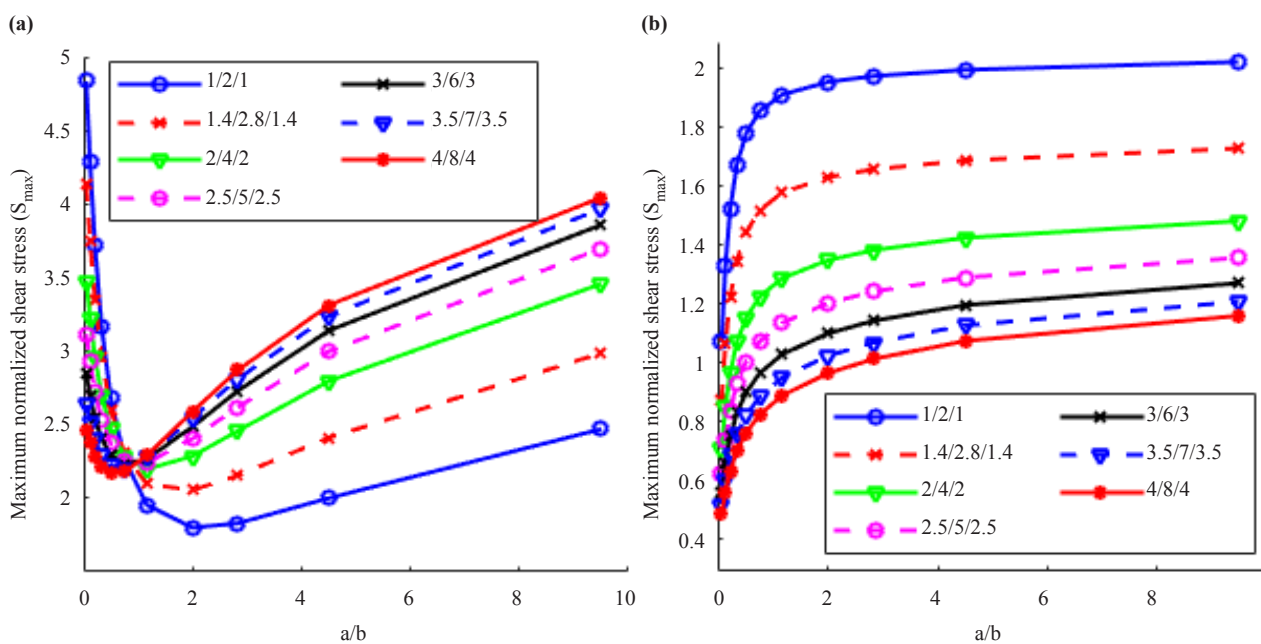
Figure 10. Evolution of the maximum normalized shear stress in terms of a/b in MADLJ for various adherent thicknesses for E_{a1}/E_{a2} = 0.137 in (a) the stiff region and (b) in the soft region

The next step consists in exploring the effect of the substrate's thickness by examining all the configurations cited in Table 5. As long as the substrate's thickness increases, the gap between the maximum stress levels in the stiff and soft regions increases on one hand while the optimal ratio a/b in the stiff region decreases as the thickness of the adherent increases.

Those aspects could be observed in graphs of Figure 10 illustrating S_{max} in the stiff and soft regions in terms of a/b

for $E_{a1}/E_{a2} = 0.137$. In Figure 10(a), for low values of a/b, the maximum stress level decreases with the increment of the adherent thickness; at a certain ratio a/b barely less than 1, the order is completely reversed and the stress increases as the adherent thickness increases. For 1-2-1 and 1.4-2.8-1.4 configurations, the optimal ratio a/b is around 2, while in 2-4-2 and 2.5-5-2.5, this ratio becomes around 1.16. The optimal ratio in 3-6-3 and 3.5-7-3.5 is found to be approximately 0.75; finally, a/b optimal scores a value of 0.5 in 4-8-4 configuration.

Table 6. Optimal and critical adhesive length ratios for $E_{a1} = 0.37$ and 0.1 GPa respectively along all the adherent thicknesses

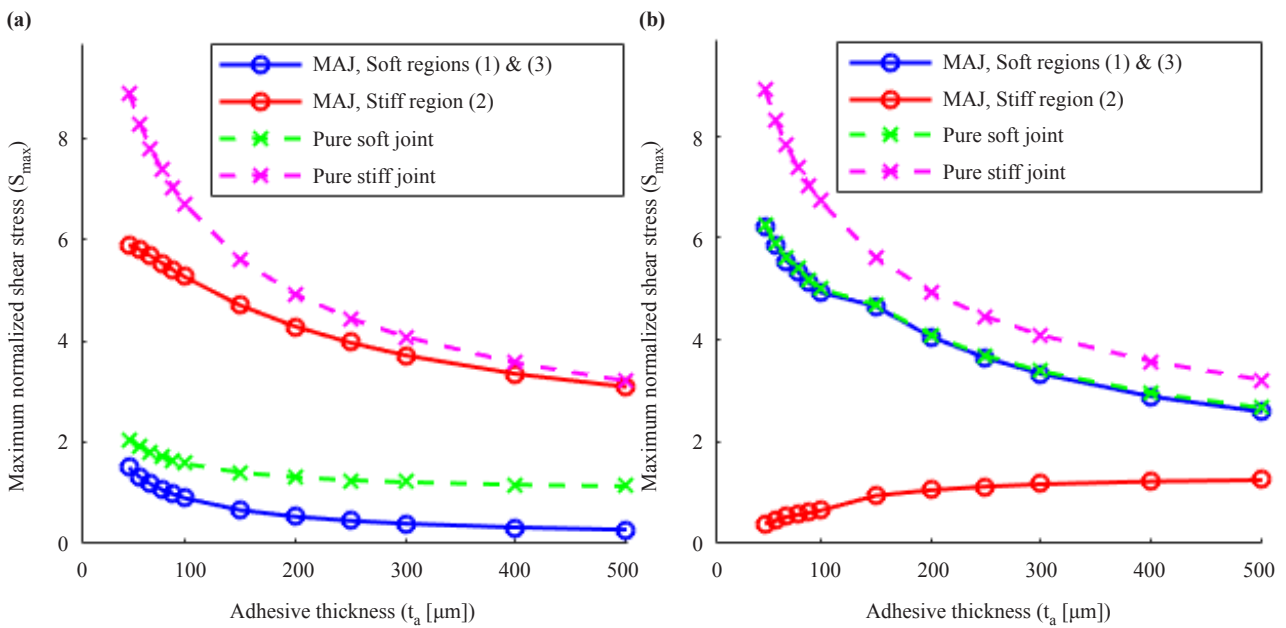| Configuration	$E_{a1}/E_{a2} = 0.137$		$E_{a1}/E_{a2} = 0.037$	
	$(a/b)_{opt}$	$(a/b)_{cr}$	$(a/b)_{opt}$	$(a/b)_{cr}$
1-2-1	2	NA	1.16	4
1.4-2.8-1.4	2	NA	0.75	2.4
2-4-2	1.16	NA	0.5	1.4
2.5-5-2.5	1.16	6.5	0.33	1
3-6-3	0.75	3.7	0.33	0.65
3.5-7-3.5	0.75	2.6	0.21	0.33
4-8-4	0.5	1.8	0.12	0.05

Another interesting aspect to be put under spot is the critical ratio a/b above which S_{max} in the stiff region in MADLJ exceeds S_{max} in a pure stiff joint: for thinner adherents, MADLJ is advantageous for the whole range of a/b as shown in Figure 9(b) for 1.4-2.8-1.4 configuration. As the substrate thickness increases, the level of maximum stress in a pure stiff joint decreases, and thus the maximum stress in MADLJ gets closer to the pure stiff joint; mathematically this critical ratio represents the intersection between the S_{max} curve of the stiff MADLJ region and S_{max} = constant in the pure stiff joint. As the thickness of the substrate increases, the critical lengths ratio decreases, as well as this critical ratio, decreases when E_{a1}/E_{a2} decreases as shown in Table 6. This observation comes in line with the previous sub-section's discussion about the existence of $E_{a1}/E_{a2})_{min}$ below which the MADLJ exhibits higher stresses than pure adhesive joint for a known lengths ratio a/b. This means that, upon the thickness of the substrates, one has the choice between selecting an appropriate modulus ratio E_{a1}/E_{a2} within the useful range in case a/b is certainly pre-defined or selecting an appropriate a/b once the adhesives moduli are already set. Table 6 summarizes the optimal and critical values of a/b for two values of E_{a1}/E_{a2}.

4.3 *Joint thickness*

In this part, the influence of the adhesive thickness on the maximum stress level in the MADLJ will be discussed and this under $E_{a1}/E_{a2} = 0.137$ and a/b = 1/3. Twelve adhesive thickness values are considered (in mm): 50, 60, 70, 80, 90, 100, 150, 200, 250, 300, 400, and 500. It should be noticed that in the original model [21], the thickness was set at 250 mm with a 1.4-2.8-1.4 configuration. Graph of Figure 11 illustrates the maximum normalized shear stress evolution along with the adhesive thickness. It could be observed that the maximum stress level in the stiff region increases to reach a maximum of 100 mm and then decreases for higher thicknesses, and for all times this maximum remains below the maximum in a pure stiff joint.
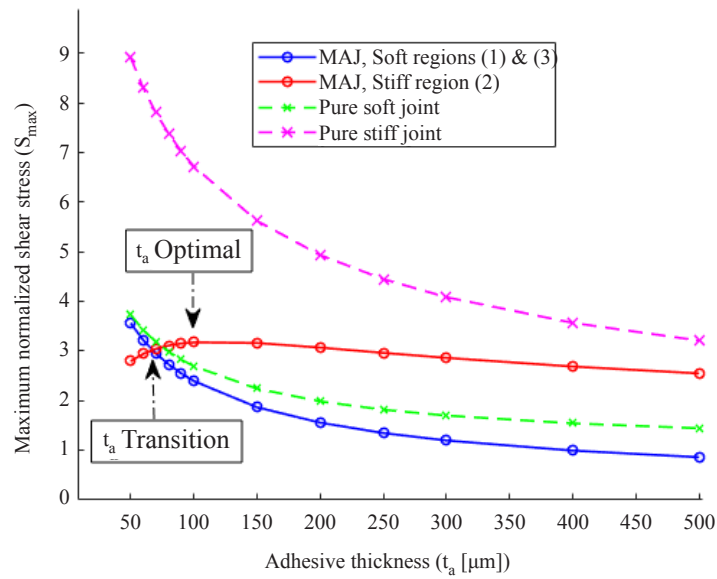
Figure 11. Evolution of the maximum normalized shear stress in terms of adhesive thickness in MADLJ, pure stiff and soft joints for 1.4-2.8-1.4 configuration for $E_{a1}/E_{a2} = 0.137$
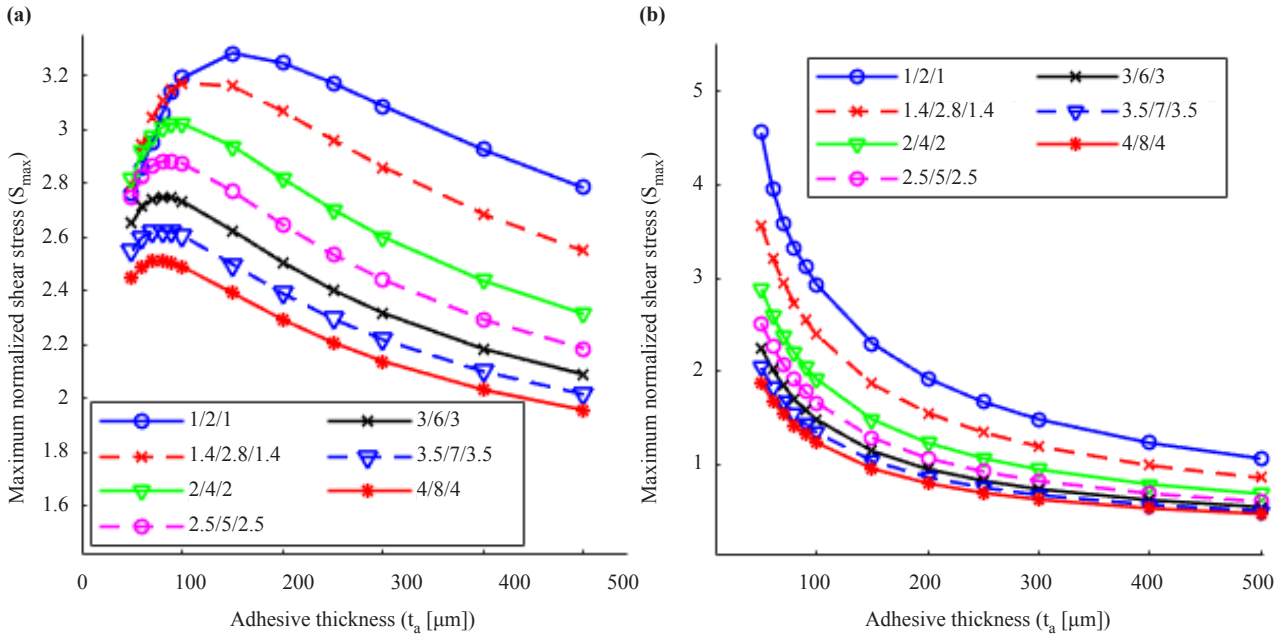

Figure 12. Evolution of the maximum normalized shear stress in terms of adhesive thickness in MADLJ, pure stiff and soft joints for 1.4-2.8-1.4 configuration for (a) $E_{a1}/E_{a2} = 0.037$ and (b) $E_{a1}/E_{a2} = 0.667$

On the other hand, S_{max} in the soft region decreases monotonically and remains slightly lower than S_{max} developed in a pure soft joint. At very low joint thicknesses S_{max} in the soft region is higher than in the stiff region and thus this group of thicknesses is to be avoided in order to obtain strong MADLJ. The transition adhesive thickness above which the maximum stress in the stiff region exceeds the soft region is about 67 mm (Figure 11). By decreasing E_{a1}/E_{a2} to 0.037, Figure 12(a) shows that the maximum stress level in the stiff region decreases monotonically with the adhesive thickness hence it does not pass anymore by a maximum. Also, the gap between the curves for stiff and soft regions

increases as E_{a1}/E_{a2} decreases such that the transition adhesive thickness disappears completely as shown in Figure 12(a). Comparing S_{max} developed in the stiff region of the MADLJ and in a pure stiff joint, the levels get closer as the adhesive thickness increases, however, they do not intersect yet in the range of the considered thicknesses.

Figure 13. Evolution of the maximum normalized shear stress in terms of the adhesive thickness in MADLJ for a variety of adherent thicknesses for $E_{a1}/E_{a2} = 0.137$ in (a) the stiff region and (b) the soft region
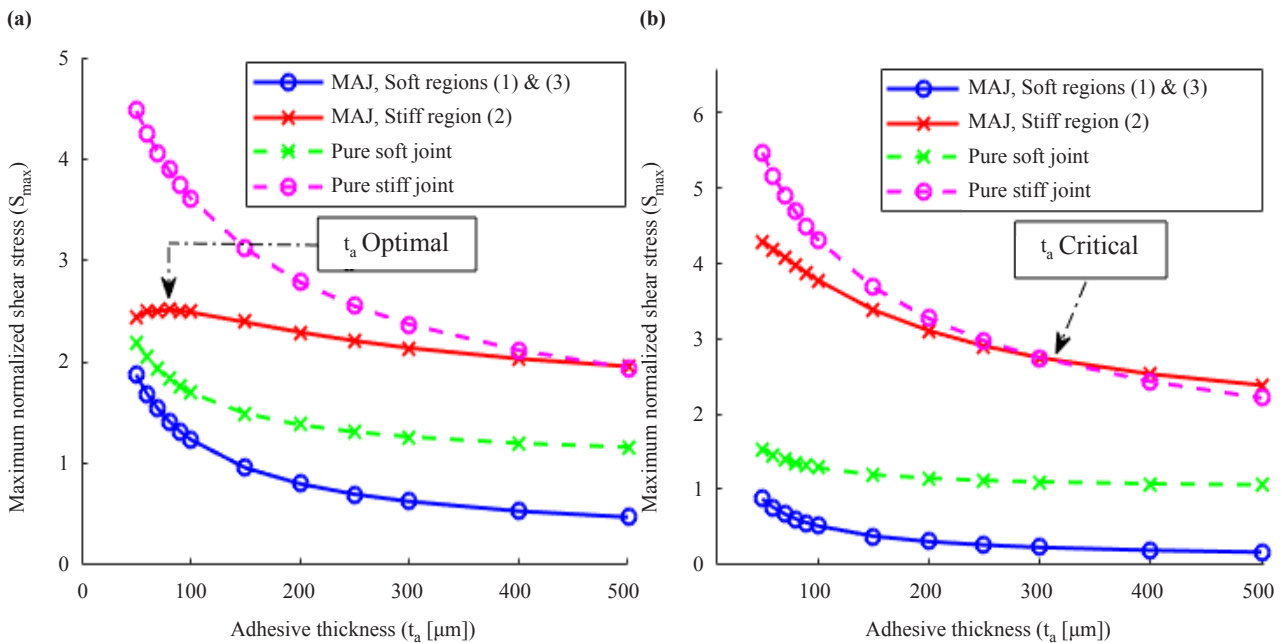
Figure 14. Evolution of the maximum normalized shear stress in terms of adhesive thickness in MADLJ, pure stiff and soft joints for (a) 4-8-4 configuration for $E_{a1}/E_{a2} = 0.137$ and (b) 3-6-3 configuration for $E_{a1}/E_{a2} = 0.037$

When E_{a1}/E_{a2} increases and gets the value of 0.667, the maximum shear stress level in the soft region becomes much higher than in the stiff region; this has been already observed in the previous sub-section (as in Figure 9(c)) since 0.667 is out of useful interval of moduli ratio. This is illustrated in Figure 14(b). One can also remark from this latter graph that S_{max} curves of the MADLJ soft regions and of the pure soft joint are tightly closed.

The next step consists of exploring the effect of the substrate's thickness by examining all the configurations starting with $E_{a1}/E_{a2} = 0.137$ and a/b = 1/3. First of all, Figure 13 shows that the maximum normalized shear stress in both stiff and soft regions decreases when the adherents' thickness increases. Moreover, when the substrate's thickness increases, the adhesive thickness maximizing the normalized shear in the stiff region decreases; the same tendency for the transition adhesive thickness is observed. From configuration 2.5-5-2.5 and above, the adhesive transition thickness becomes less than 50 mm and thus is outside the considered range.

In addition, for all configurations, the maximum stress level in a pure stiff joint remains always above this maximum developed in the stiff region of the MADLJ; the same applies to the soft case. However, as the substrate thickness increases, the gap between S_{max} in the soft region of the MADLJ and the pure soft joint increases along with the adhesive thickness. This gap decreases for the stiff case; they converge exactly in the 4-8-4 region at the highest adhesive thickness considered, which is 500 mm as shown in Figure 14(a). For $E_{a1}/E_{a2} = 0.037$, similar tendencies have been observed for all configurations as those of the original one 1.4-2.8-1.4. However, under that low ratio of E_{a1}/E_{a2} critical adhesive thicknesses appear, above which S_{max} in the stiff MADLJ region exceeds S_{max} in a pure stiff joint; the values of the critical thickness decrease as the adherent thickness increases. Figure 14(b) shows, as an example, the critical adhesive thickness for the 3-6-3 configuration. All the remarkable values of adhesive thickness are summarized in Table 7. For $E_{a1}/E_{a2} = 0.667$, similar tendencies have been observed for all configurations as those for the original one 1.4-2.8-1.4.

Table 7. MADLJ critical and optimal adhesive thicknesses at low Young's modulus ratios

Configuration	$E_{a1}/E_{a2} = 0.137$		$E_{a1}/E_{a2} = 0.037$
	$t_{a,opt}$ (mm)	$t_{a,tr}$ (mm)	$t_{a,cr}$ (mm)
1-2-1	150	81	NA
1.4-2.8-1.4	100	67	NA
2-4-2	100	51	446
2.5-5-2.5	90	NA	396
3-6-3	80	NA	300
3.5-7-3.5	80	NA	250
4-8-4	80	NA	220

4.4 *Combined parametric analysis*

Taking into account the results established in 4.2 and 4.3, one may reduce the range of values of the ratio a/b and adhesive thickness (Table 8) leading to a MADLJ advantageous technique. Then useful range consisting of $E_{a1}/E_{a2})_{min}$ and $E_{a1}/E_{a2})_{tr}$ will be determined for all adherent thicknesses' configurations in order to deduce some tendencies. For each adhesive thickness stated in Table 8, the 6 values of the ratio a/b were varied such that results similar to those stated in Table 4 are obtained, and this is for all the adherents' configurations. It should be noticed that a couple of calculated

values $E_{a1}/E_{a2})_{min}$ might be theoretical (too low) meaning that the practical lower boundary of the useful moduli ratio is quite open in that case.

Table 8. MADLJ useful values of adhesive thicknesses and adhesive length ratios

| t_a (mm)	150	200	250	300	400	500
a/b	0.12	0.21	0.33	0.5	0.75	1.16

As a first observation, as seen also in Table 4, for a well-known adhesive thickness and lengths ratio a/b, both $E_{a1}/E_{a2})_{min}$ and $E_{a1}/E_{a2})_{tr}$ increase with the increment of the substrate's thickness while the maximum stress level at those ratios decreases. This evolution could be seen in a clearer manner in the graph of Figure 15(a).

Examining the effect of the adhesives lengths ratio a/b, for the original model (1.4-2.8-1.4; $t_a = 250$ mm), it could be remarked that the increase of the ratio a/b leads to an increase of $E_{a1}/E_{a2})_{min}$, a decrease of $E_{a1}/E_{a2})_{tr}$ and thus the range of useful Young's moduli is also reduced, reaching a maximum reduction of 3 times approximately for the adopted values in this study. Furthermore, the maximum normalized stress at the transition point decreases when the ratio a/b increases where the largest drop reaches 34%. All those observations are illustrated in Figure 15(b).

The next analysis consists in exploring the effect of the adhesive thickness on the useful interval of Young's moduli ratio, for configuration 1.4-2.8-1.4 and for a/b = 1/3. The results are depicted in the graph of Figure 15(c). Indeed, increasing the joint's thickness leads to a simultaneous increase of $E_{a1}/E_{a2})_{min}$ and $E_{a1}/E_{a2})_{tr}$, the latter reaching a maximum increment of 74%. The maximum normalized stress at transition follows the same trend and decreases as long as the joint gets thicker, the largest difference for the adopted values reaches 29%.

Following the trends of all the aforementioned observations, one can remark that those apply also to all the possible combinations of parameters. For the sake of brevity, one may illustrate, as examples, the evolution of $E_{a1}/E_{a2})_{min}$ and $S_{max, upper}$ in Figures 16 and 17 respectively, and this only for the thinnest (1-2-1) and the thickest (4-8-4) substrates.

(a)

(b)

(c)
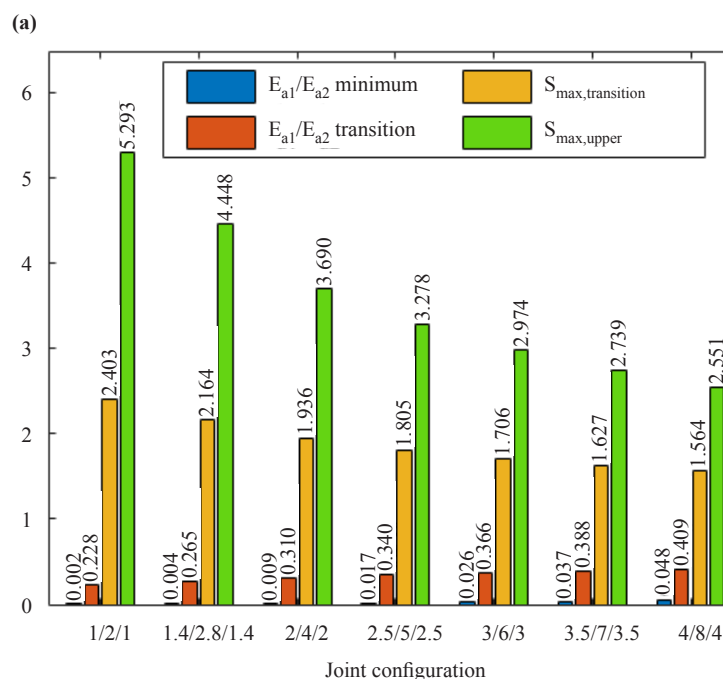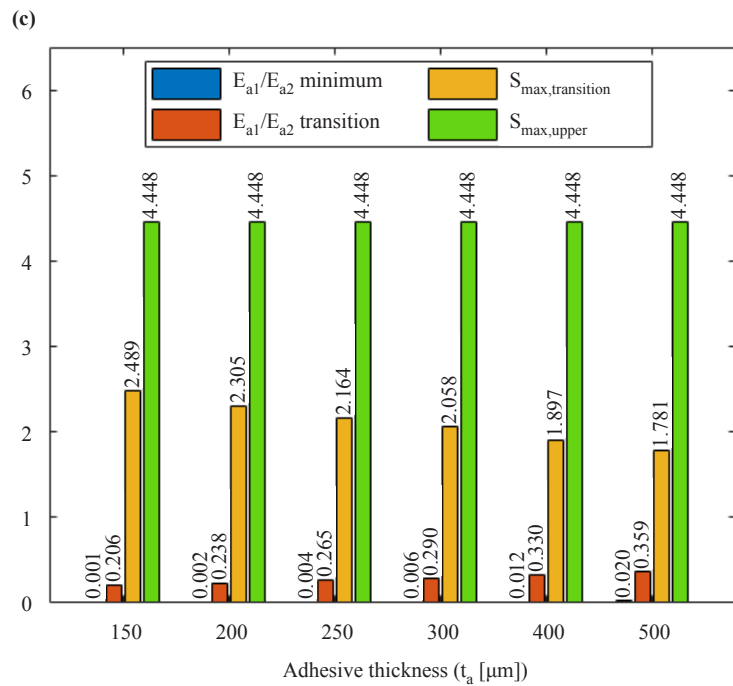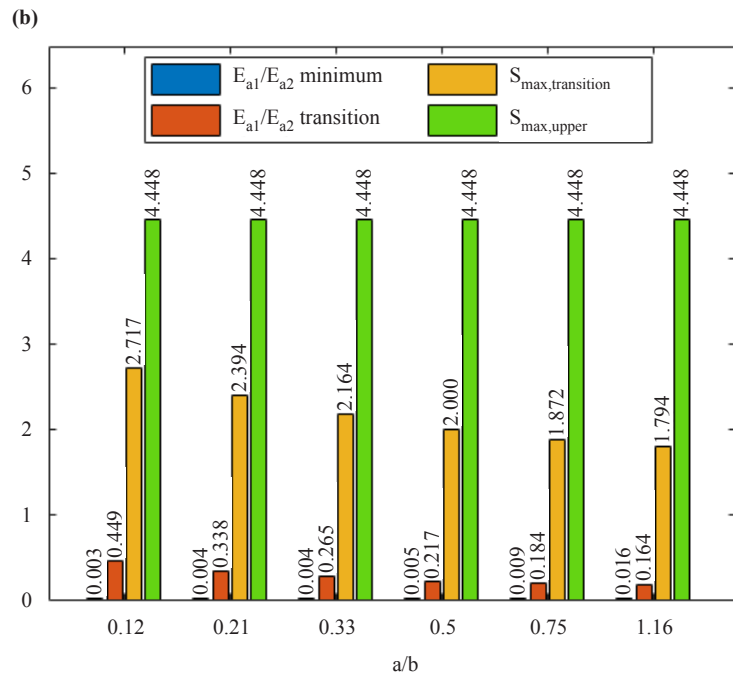
Figure 15. Evolution of the useful Young's moduli ratio range and the corresponding maximum normalized shear stresses in MADLJ in terms of (a) adherents' thicknesses for a/b = 1/3 and t_a = 250 mm, (b) of a/b for 1.4-2.8-1.4 configuration and t_a = 250 mm and (c) of adhesive thickness for 1.4-2.8-1.4 configuration and a/b = 1/3

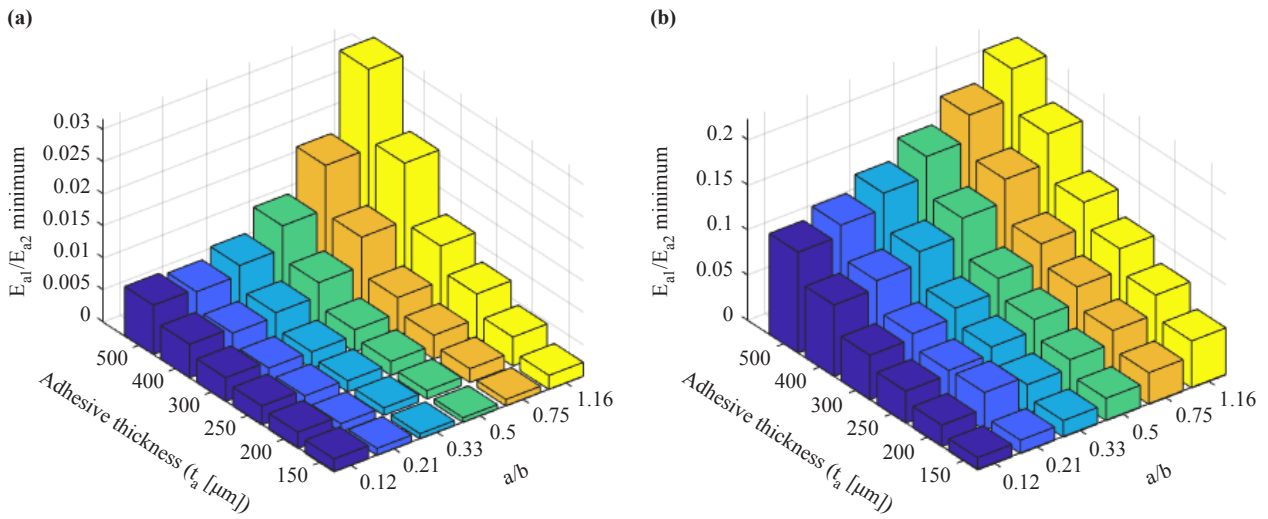(a)   (b)

Figure 16. Influence of both adhesive lengths ratio a/b and adhesive thickness on $E_{a1}/E_{a2})_{min}$ for (a) 1-2-1 and (b) 4-8-4 configurations
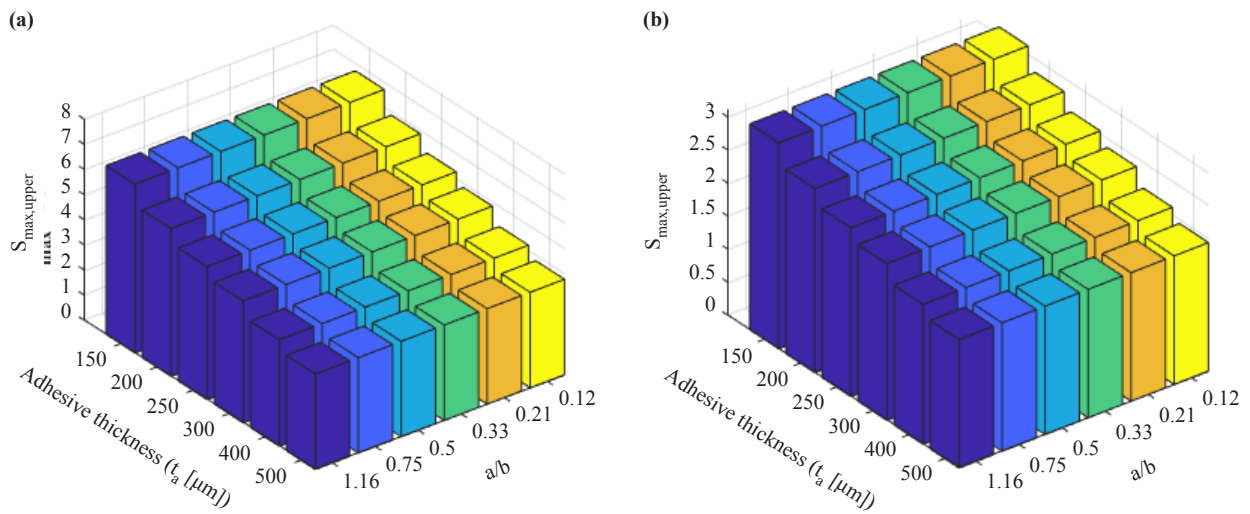
(a)   (b)

Figure 17. Influence of both adhesive lengths ratio a/b and adhesive thickness on $S_{max, upper}$ for (a) 1-2-1 and (b) 4-8-4 configurations

5. Conclusion

A closed-form expression of adhesive shear stress in a MADLJ based on an improved shear lag model has been developed and validated. This has saved an enormous time to carry out the parametric study discussed in this work if it would have been performed experimentally or even through numerical simulations. However, it should be reminded that the behavior of the adhesive is considered elastic linear, and the shear stress was considered to be unchanged through the thickness of the adhesive. Many key points could be concluded from this work:

• The MADLJ technique is not advantageous over pure adhesive joints in absolute but just in a useful interval $[E_{a1}/E_{a2})_{min}; E_{a1}/E_{a2})_{tr}]$. This useful interval varies considerably with the geometry of the structure; namely the adhesive and adherents' thicknesses and the adhesives' lengths ratio a/b.

• In the useful interval $[E_{a1}/E_{a2})_{min}; E_{a1}/E_{a2})_{tr}]$, and for a determined adhesive and adherent thickness, the maximum shear in the stiff MADLJ region passes through a minimum at a certain optimal ratio a/b$)_{opt}$.

• When the adherent's thickness increases, a critical value of $(a/b)_{cr}$ is recorded, after which, the maximum stress in MADLJ exceeds the one in the pure stiff joint. This critical value decreases when the adherent thickness increases and E_{a1}/E_{a2} decreases in the useful interval.

•For moderate values in $[(E_{a1}/E_{a2})_{min}; (E_{a1}/E_{a2})_{tr}]$ and for a determined a/b, the maximum shear in the stiff MADLJ region passes through a maximum at an optimal thickness while in the soft region it decreases continuously. After a certain transition thickness, the maximum stress in the stiff region exceeds the one in the soft region.

•The optimal, transition, and critical adhesive thicknesses decrease with the increase of the adherent thickness.

•For a well-known adhesive and adherent thickness, $E_{a1}/E_{a2})_{min}$, $E_{a1}/E_{a2})_{tr}$, and S_{max_tr} decrease when a/b increases.

•For a well-known a/b and adherent thickness, $E_{a1}/E_{a2})_{min}$, $E_{a1}/E_{a2})_{tr}$ increase while S_{max_tr} decreases as long as the joint's thickness increases.

Finally, to select any mechanical and geometrical configuration of a MADLJ, one must not only look at the maximum stress level in each region, but also the strength of each adhesive. As stated in [24], one should compare the ratio $S_{max\_stiff}/S_{max\_soft}$ developed in the mixed joint to the strengths ratio of stiff (brittle) to soft (ductile) adhesive in order to either prevent yielding failure of the mixed-adhesive joint or even to select a pure adhesive joint when it is more advantageous.

Acknowledgements

Conflict of interest

The authors declare no competing financial interest.

References

[1] Z. D. Li, Z. G. Wang, X. X. Wang, and W. Zhou, "Bending behaviour of sandwich beam with tailored hierarchical honeycomb core," *Thin-Walled Structures*, vol. 157, pp. 107001, 2020.

[2] Z. G. Wang, Z. D. Li, and W. Xiong, "Experimental investigation on bending behavior of honeycomb sandwich panel with ceramic tile-face sheet," *Composites Part B: Engineering*, vol. 164, pp. 280-286, 2019.

[3] Z. G. Wang, Z. P. Lei, Z. D. Li, K. Yuan, and X. X. Wang, "Mechanical reinforcement mechanism of a hierarchical Kagome honeycomb," *Thin-Walled Structures*, vol. 167, pp. 108235, 2021.

[4] O. Volkersen, "Die Nietkraftverteilung in zugbeanspruchten Nietverbindungen mit konstanten Laschenquerschnitten," *Luftfahrtforschung*, vol. 15, pp. 41-47, 1938.

[5] M. Goland, and E. Reissner, "The stresses in cemented joints," *ASME Journal of Applied Mechanics,* vol. 11, no. 1, pp. A17-A27, 1944.

[6] L. J. Hart-Smith, "Adhesive-bonded double-lap joints," Technical Report. Langley Research Center Hampton, Virginia, NAS1-11234 23366, 1973.

[7] D. J. Allman, "A theory for elastic stresses in adhesive bonded lap joints," *Quarterly Journal of Mechanics and Applied Mathematics,* vol. 30, no. 4, pp. 415-436, 1977.

[8] D. A. Bigwood, and A. D. Crocombe, "Elastic analysis and engineering design formulae for bonded joints," *International Journal of Adhesion and Adhesives*, vol. 9, no. 4, pp. 229-242, 1989.

[9] D. A. Bigwood, and A. D. Crocombe, "Non-linear adhesive bonded joint design analyses," *International Journal of Adhesion and Adhesives*, vol. 10, no. 1, pp. 31-41, 1990.

[10] A. D. Crocombe, and D. A. Bigwood, "Development of a full elasto-plastic adhesive joint design analysis," *The Journal of Strain Analysis for Engineering Design*, vol. 27, no. 4, pp. 211-218, 1992.

[11] R. X. Wang, J. Cui, A. N. Sinclair, and J. K. Spelt, "Strength of adhesive joints with adherend yielding: I. Analytical model," *The Journal of Adhesion*, vol. 79, no. 1, pp. 23-48, 2010.

[12] R. D. Adams, and V. A. Mallick, "A method for the stress analysis of lap joints," *The Journal of Adhesion*, vol. 38,

no. 3-4, pp. 199-217, 1992.

[13] R. D. Adams, J. Comny, and W. C. Wake, *Structural Adhesive Joints in Engineering*. 2nd ed. Springer Netherlands, 1997.

[14] M. Y. Tasi, D. W. Oplinger, and J. Morton, "Improved theoretical solutions for adhesive lap joints," *International Journal of Solids and Structures*, vol. 35, no. 12, pp. 1163-1185, 1998.

[15] G. Challita, "The influence of a void on the behavior of a double lap bonded joint," in *Advances in Engineering Research*, V. M. Petrova, Ed. Nova Science Publishers Inc, 2018, pp. 81-118.

[16] G. Li, "Elastic analysis of closed-form solutions for adhesive stresses in bonded single-strap butt joints," *Journal of Mechanics of Materials and Structures*, vol. 5, no. 3, pp. 409-426, 2010.

[17] Y. Frostig, O. T. Thomsen, and F. Mortensen, "Analysis of adhesive-bonded joints, square-end, and spew-fillet-high-order theory approach," *Journal of Engineering Mechanics*, vol. 125, no. 11, pp. 1298-1307, 1999.

[18] R. D. Adams, S. H. Chambers, P. J. A. Del Strother, and N. A. Peppiatt, "Rubber model for adhesive lap joints," *The Journal of Strain Analysis for Engineering*, vol. 8, no. 1, pp. 52-57, 1973.

[19] C. Raphael, "Variable-adhesive bonded joints," *Applied Polymer Symposium*, vol. 3, no. 3, pp. 99-108, 1966.

[20] L. F. M. da Silva, "Technology of mixed adhesive joints," *Advanced Structural Materials*, vol. 6, pp. 283-309, 2010.

[21] G. J. Broughton, and M. D. Fitton, "Science of mixed-adhesive joints," *Advanced Structural Materials*, vol. 6, pp. 257-281, 2010.

[22] L. F. M. da Silva, and M. J. C. Q. Lopes, "Joint strength optimization by the mixed-adhesive technique," *International Journal of Adhesion and Adhesives*, vol. 29, no. 5, pp. 509-514, 2008.

[23] I. Pires, L. Quintino, J. F. Durodola, and A. Beevers, "Performance of bi-adhesive bonded aluminum lap joint," *International Journal of Adhesion and Adhesives*, vol. 23, pp. 215-223, 2003.

[24] M. D. Fitton, and G. J. Broughton, "Variable modulus adhesives: An approach to optimised joint performance," *International Journal of Adhesion and Adhesives*, vol. 25, no. 4, pp. 329-336, 2004.

[25] S. Srinivas, "Analysis of bonded joints," Langley Res. Cent., Hdmpton, Va 23665 Natl. Aeronaut., AMD Sp. Administration Washington 5C, NASA, TN D-7855, 1975.

[26] J. C. das Neves, L. F. M. da Silva, and R. D. Adams, "Analysis of mixed adhesive bonded joints Part I: Theoretical formulation," *Journal of Adhesion Science and Technology*, vol. 23, no. 1, pp. 1-34, 2012.

[27] J. C. das Neves, L. F. M. da Silva, and R. D. Adams, "Analysis of mixed adhesive bonded joints Part II: Parametric study," *Journal of Adhesion Science and Technology*, vol. 23, no. 1, pp. 35-61, 2012.